POLITECNICO DI TORINO

Master's Degree in Automotive Engineering

Master's Degree Thesis

Aerial Cargo Vehicle for Last Mile Delivery

Concept Design & CFD Validation of Urban-Air-Mobility Winglet-Featured Wings

Supervisor

Prof. Maria Pia Cavatorta

Student

Mohamad Hamze

July 2023

Summary

Urban Air Mobility (UAM) is an emerging technology primarily used for passenger transport, driven by the growing awareness of the need to alleviate traffic congestion and reduce emissions. While UAM is expected to enter the market by 2030, with some aerial passenger transport projects already under development in 2023, there is limited information available regarding its potential application in cargo transport. Therefore, the purpose of this thesis is to propose a preliminary conceptual design for a UAM solution specifically tailored for last-mile delivery. This solution, similar to drones but with enhanced capabilities, aims to fulfill multiple orders by utilizing a main aerial platform equipped with small drones for parcel handling, enabling delivery to the end user via air transportation.

The thesis begins by providing a description of the solution's context, as well as its function and integration within the business-to-consumer (B2C) framework. The initial topic of automated transshipment of goods originated from the IDEEA 2023 international project, which focuses on future mobility solutions. The outcome of this project is the Mother&babydrones Shuttle (MbdS), which serves as the basis for the proposed solution.

The development of this solution was driven by comprehensive market research, which led to the selection of suburban areas as the target location. The goal is to connect distribution centers situated in outlying areas with the detached houses of users in commuter towns. This approach ensures efficient last-mile delivery in a suburban setting.

The second part of the thesis focuses on the numerical aspect, specifically the geometry and design of the preliminary aircraft's wing shape. Through a series of computational fluid dynamics (CFD) simulations, various wing configurations, including different winglet designs, were analyzed to determine the configuration that minimizes drag during cruising. The objective of this section was to validate the effectiveness of utilizing winglet devices in a four-winged urban cargo aircraft.

By addressing the gap in knowledge regarding UAM's application in cargo transport and providing a preliminary conceptual design for last-mile delivery, this thesis aim contributes to the growing field of urban air mobility and its potential impact on logistics and transportation systems.

Acknowledgment

I would like first to thank all my team members in the IDEEA 2023 project who participated in the development of this work. The delivery concept subject of this thesis would not have been possible without the valuable contributions of the Korean, Chinese and Italian members in our team.
Above all, I would like to express my sincere gratitude to the original author of the idea and the brilliant designer Choe (Alex), who designed completely the aerial cargo vehicle concept presented in this thesis. All the 3D rendering of the solution was developed by him.
Particular thanks to Yuri for her constant initiatives in teamwork organization and full availability in developing this project. The mechanical system calculation was majorly developed by her and other Korean members.
Very special thanks to Jinghan, the visionary member of our team who generated the CAD drawings of the warehouse, for her dedication in driving the team forward to develop a futuristic solution. The warehouse planning part was a collaborative effort between me and her.
I would like to thank Huanxia as well for his valuable support and contribution in the development of the winglet validation part.
I cannot miss extending my sincere appreciation to my supervisor, Professor Maria Pia, for her undivided availability and support, and for granting me the opportunity to be part of this project and undertake the development of my thesis. It was an honour to work with you.

At this stage of my life, I would like to express my gratitude to my family for standing by me throughout my academic journey.
I would like proudly to say to my father Fathi, you are a lifetime lesson for me. I am blessed and proud to have learned my wisdom and strength from a great man like you.
In particular, I want to extend my deepest gratitude to my beloved older brother, Fawzi, for his support in enabling me to complete my study in Italy. Your presence and support in this period in my life have meant the world to me, and I am truly grateful to have you in my life as a brother, close friend and partner.
I would like to thank my adored Mother, your prayers are always leading the doors of success for me. I want to thank my compassionate brother Farouk, that always wanted to see me an engineer. I am proud to have you my big brother. I would like to thank my sister Farah, whom I have grown up seeing as my second mother, for cheering always for me. And finally I want to thank my sweetheart sister Jana for her unlimited love. I am blessed to have you all in my life.

Contents

List of Figures

Chapter 1

Introduction

This thesis aims to propose a novel design concept for last mile delivery utilizing unmanned aerial vehicle. In this thesis, it is referred to as the *Mother&BabyDrones Shuttle(MbdS)*. The proposed concept aims to address the challenges associated with last mile delivery by introducing an aerial cargo vehicle equipped with multiple drones loaded with parcels.

On the other side, this delivery aerial vehicle incorporates a novel wing configuration featuring winglets to enhance the aircraft's cruising performance. A thorough selection of the winglet angle has been made through a series of CFD simulations, ultimately validating the chosen winglet angle that improve the overall aerodynamic performance of the cargo shuttle.

The project was born thanks to an interdisciplinary collaboration of different universities involved in IDEEA 2023 Competition.
IDEEA is a community of designers and engineers from different universities that organizes yearly academic competitions between international universities in themes related to mobility. The theme of this year, sponsored by Volkswagen, was Automated Transshipment of Goods(AToG) : Delivery Mobility Solution for 2040. With the target of designing a smart mobility solution for the future, that deals with the challenges associated with last mile delivery in suburbans cities, the concept has been developed through a shared work between automotive engineers and designers.

Delivery Urban Air Mobility (UAM) are autonomous flying system that have the potential to revolutionize package and goods transportation by ensuring swift delivery to users' homes without human involvement. With a variety of operational modes and delivery approaches, UAM concepts are conceived to navigate urban skies shifting last-mile logistics from roads to air. This visionary approach not only mitigates traffic congestion but also reduces emissions, paving the way for a more sustainable future.

The growing prevalence of the internet and the rapid growth of the e-commerce sector have led to an upsurge in online shopping, consequently creating a greater need for more effective and efficient methods of product delivery to customers. As a result, companies have embraced various delivery services. The

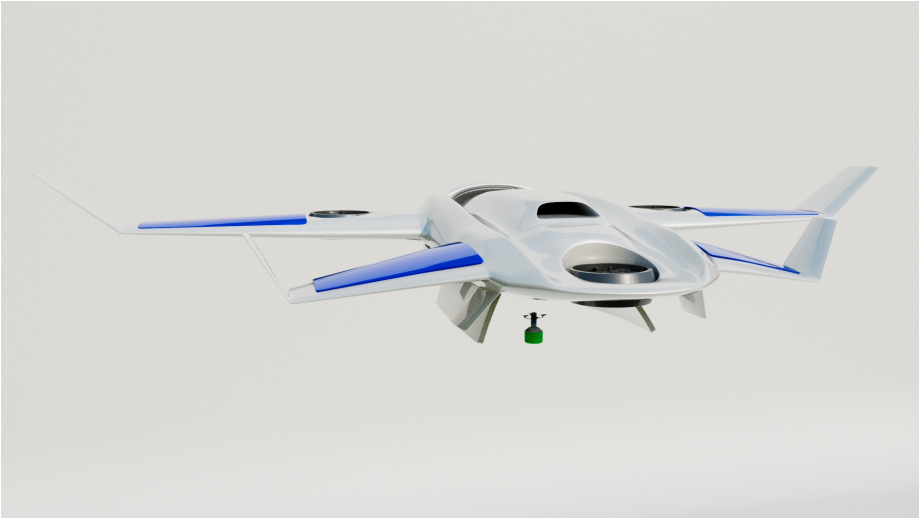

Figure 1.1: Mother&BabyDrones Shuttle concept for last mile delivery

aim was to develop a novel and improved delivery solution tailored for future environment surpassing from the limitations and drawbacks of existing systems

1.1 Background

As of 2023, last-mile delivery presents numerous challenges when conducted through traditional means involving third-party providers (3PL), such as Amazon and DHL, who predominantly rely on manned vehicles for goods transportation. Even though these vehicles may be fully electric and emission-free, they still contribute, to varying degrees, to traffic congestion. Moreover, the exponential growth observed in the online delivery market is compelling companies and key stakeholders (such as Amazon) to explore alternative methods involving unmanned vehicles, such as delivery robots, that operate without direct human involvement. While, in the case of Unmanned Aerial Vehicles (UAVs) like drones, the objective extends beyond meeting the surging demand for orders; it aims to attain the utmost customer satisfaction in terms of delivery speed, accuracy, and safety.

The concept of Urban Air Mobility, defined as an air transportation system for passengers and cargo in and around urban environments, has gained significant attention in recent years, with numerous industry players, regulatory bodies, and research institutions exploring its potential. The UAM concept enables individuals to utilize aerial transportation within urban environments. However, existing literature and reviews predominantly concentrate on UAM applications for passenger transportation, as they greatly outnumber those for cargo transportation. In fact, cargo transportation leveraging UAM is often

simply referred to as "drones". Hence, the concept of "Mother&Baby Drones Shuttle" described broadly in this chapter and further elaborated in subsequent chapters, aims to fill this gap and propose an upgraded concept of drones delivery that is designed specifically to surpass the conventional last mile delivery fulfillment limitations associated with Automated Transshipment of Goods such as ADV (Autonomous Delivery Vehicle) or drones

In this section, based on a comprehensive review of existing literature, the significance of last mile delivery and the associated challenges will be examined. Additionally, an extensive overview of the Urban Air Mobility (UAM) market will be provided, including examples from current European UAM projects. This will contribute to a better understanding of UAM regulations in Europe and the US, as well as the environmental benefits it offers.

1.1.1 Last-Mile Delivery

The final stage of the logistics chain, known as last mile delivery or the "final leg," represents with the highest complexities as it directly influences the customer experience and determines the overall success of the delivery process. It accounts for a cost ranging from 13% to 73% of the total distribution cost.[1]

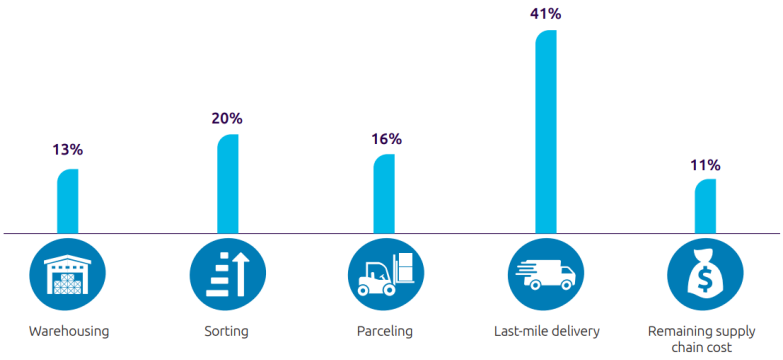

Figure 1.2: Last-mile delivery contribution to the total cost of supply chain [2]

The significance of last mile delivery in ensuring customer satisfaction is paramount, particularly in response to the growing demand for expedited and unrestricted delivery of various products. The food and grocery markets have seen monumental growth in the past decade. The global food delivery market tripled over the previous five years to be currently valued at 150 billion$, with the US market alone having doubled in the past two years.[3]

However, conventional delivery methods have negative implications for the environment, traffic congestion, and public safety.In Shanghai, there is one fatal accident involving a delivery driver every two and a half days. [4]

With regard to the last mile delivery implications for traffic congestion, the

top 25 most congested US cities are projected to experience a loss of over 480$ billion within the next decade due to increased fuel consumption, time wastage, and carbon emissions.[3]

Given the importance and complexity of this logistics segment, the trend is clear towards automated last mile delivery fulfillment solutions, such as ADV (Autonomous Delivery Vehicles) and Drones. However, these methods are not flawless and raise future concerns regarding their current implementation.
Delivery robots and autonomous vehicles reduce CO2 emissions and have less noise emission compared to drones. However, if delivery robots utilize roads for transportation, it can potentially lead to increased traffic congestion. Similarly, if delivery robots use sidewalks for delivery within cities, concerns arise regarding their interaction with pedestrians and the challenges they may face in navigating crowded sidewalks. Hence, it is crucial to address the problem of last-mile delivery without compromising other factors, such as traffic congestion and pedestrian safety.

This necessity highlights the importance of transitioning last-mile delivery operations from ground to air, establishing a new aerial network for efficient last-mile delivery. Utilizing Unmanned Aerial Vehicles (UAVs) or drones in the delivery process offers advantages, such as avoiding increased congestion in urban areas and reducing CO2 emissions.

On the other hand, it is crucial to recognize the limitations associated with current delivery drones. These drones are often constrained in terms of carrying capacity, as they are typically designed for single-user trips and have restrictions on the weight of cargo they can transport. Furthermore, they often have limited flight endurance and working time.[1]

To meet these future demands, the solution required must be sustainable, contributes less to traffic congestion, has moderate interaction with citizens or pedestrians, and can achieve delivery quickly, without any restrictions on weight or travel distance. Achieving this requirements demands a revolutionary-unconventional concept of Automated Transshipment of Goods (AToG) that surpasses robots or drones. Currently, there is no literature describing a new concept design under these requirements. This is what separate the future delivery concept described here, t*he Mother&Baby shuttle*, the *mother* ship of modular drones equipped with cargo, that can achieve more delivery orders, without restriction to travel distance or weight limit, designed as an UAM (Urban Air Mobility) vehicle

1.1.2 Urban-Air-Mobility

Urban Air Mobility (UAM) is the use of small, highly automated aircraft to carry passengers or cargo at lower altitudes in urban and suburban areas which have been developed in response to traffic congestion.
The term encompasses a range of existing and emerging technologies, including traditional helicopters, vertical-takeoff-and-landing aircraft (VTOL), electrically propelled vertical-takeoff-and-landing aircraft (eVTOL), and unmanned aerial vehicles (UAVs).

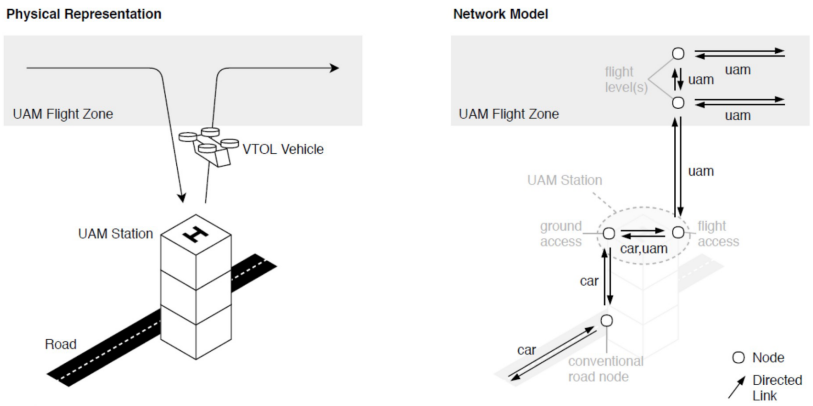

Figure 1.3: UAM Network Model
[5]

These aircraft are distinguished by their utilization of multiple electric-powered rotors or fans for both lift and propulsion, coupled with fly-by-wire systems for precise control.

As for the infrastructure needed, the Vertiports or Vertistops shown in Figure 1.3, are dedicated VTOL platforms required for taking-off and landing operation of UAM. [6]

Market Analysis

Many OEMs are leading in Europe, due to the fact that the development of new mobility technologies is being spurred by the increasing strain of traffic congestion. In Italy, in particular, noteworthy projects such as "Jaunt" and "Walle" have emerged, with "Jaunt" being currently in the Design Stage and projected to enter the market in 2026.[7]

The estimated market size of UAM in Europe, including R&D, vehicle manufacturing, operations and infrastructure construction, will be approximately 4.2 Billion Euros in 2030, which represents almost one third of the global market and hints at the opportunity that this industry may offer for Europe. The estimated market size may create or sustain approximately 90,000 jobs in 2030, based on labour spending for constructing related infrastructure and operating the UAM. If we visualise what this market size would mean for the Paris metropolitan area in terms of UAM aircraft, the estimates range from approximately 3,000 to 3,500 UAM aircraft for passenger and cargo transport in 2030. In this estimate, UAM passenger aircraft represent the smallest part with numbers between 160 and 180, whereas the estimates for the UAM cargo aircraft and delivery drones range from 2,840 to 3,300."[7]

In the US, a market study commissioned by NASA predicts a near-term demand in the U.S. of 55,000 daily trips for air taxis and airport shuttles, served

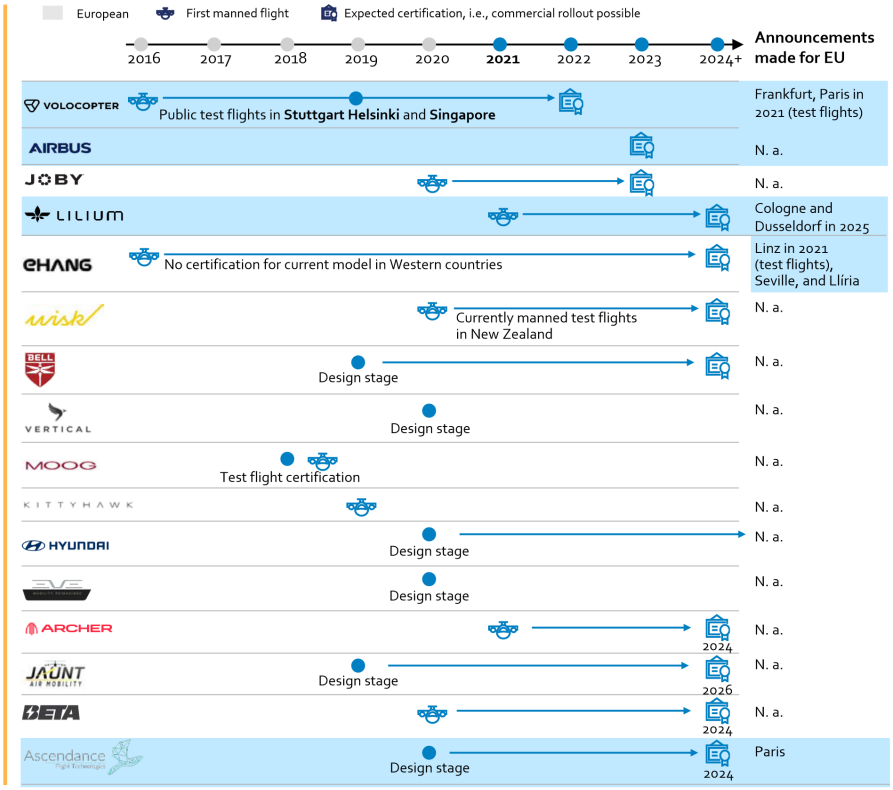

Figure 1.4: European UAM Projects
[7]

Figure 1.5: UberAir

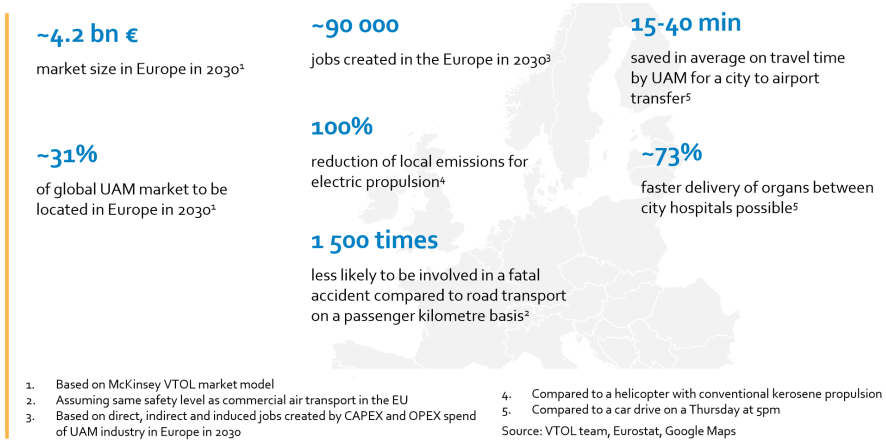

Figure 1.6: UAM Potential in Europe
. [7]

by 4100 aircraft.[6]

According to Gartner's Hype Cycle, a framework used to forecast and explain the general path a technology take over time[8], UAM technology is still in the so-called innovation trigger phase, but are expected to reach the peak of inflated expectations soon.[6]
The plateau of productivity that follows the trough of disillusionment and slope of enlightenment is said to be reached within the next five to ten years.[6]

Examples

One example of UAM for intra- and inter- urban passenger transport solution is UberAir. UBER stipulates a design mission range of about 95 km and a reserve range of almost10 km at a minimum cruise speed of 240 km/h. Cruise altitude is set to 300 m above ground level (AGL). A required payload of 500 kg is specified for four passengers. [6]

In a case similar to the "Mother&Baby Drones Shuttle", Amazon.com have already patented a first "flying-warehouse" in 2017.[9]

Regulations

Corresponding regulations for certification are currently being considered in particular by the European Aviation Safety Agency (EASA) and the US Federal Aviation Administration (FAA). The number of persons on board is limited to five and the maximum take-off mass is set to 2000 kg.

The first proposal of EASA in the Special Condition Vertical Take-Off and Landing Aircraft (SC-VTOL-01) from July 2019 (SC-VTOL-01/02.07.2019), based on the CS-23 construction and certification regulations, refers to safety

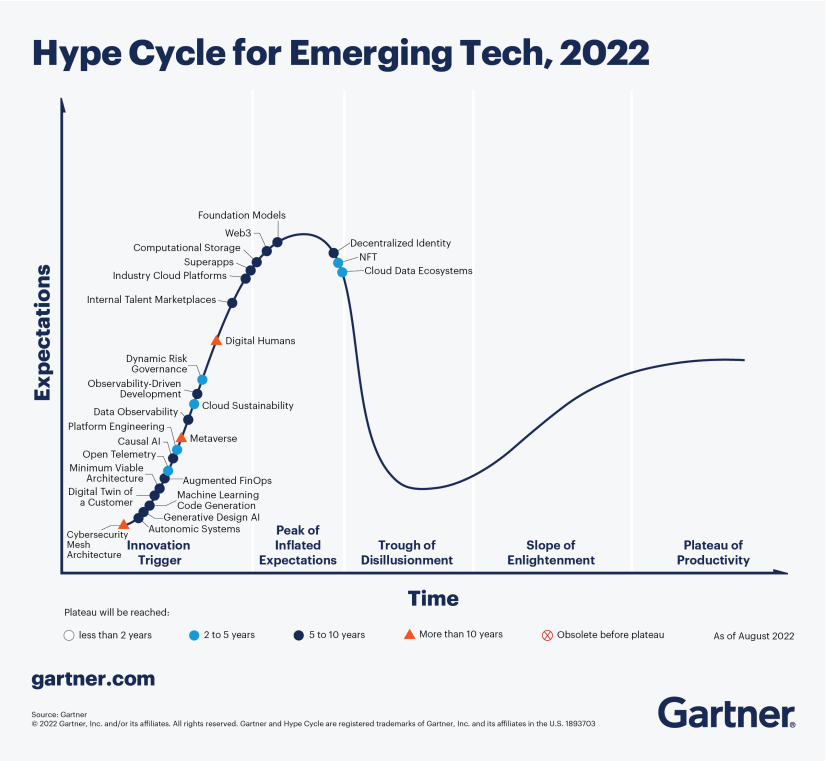

Figure 1.7: Gartner Hype Cycle for Emerging Technologies 2022 [6]

standards comparable to those applicable to smaller commercial aircraft. In addition, for use over densely populated areas or in commercial passenger transportation, the design must ensure that the aircraft can continue to fly and land safely even after a critical malfunction in the propulsion system.[6].

However, the time-frame until which European approval regulations for autonomous and pilot-less UAMs are available is still open and may probably take several years.

Other companies reviewed within the cargo use case are Amazon and Volodrone. Amazon have already achieved operational certification in US.

Eco-Friendliness

First investigations regarding greenhouse gas emissions(GHG) indicate that under certain boundary conditions, VTOL aircraft for three or more passengers produce fewer emissions than combustion engine powered automobiles and even battery powered cars.[6]

Considering for instance, a 100-km mission and assuming an average occupancy of 1.54 passengers for ground based vehicles, the emissions per passenger

Figure 1.8: Amazon flying warehouse future concept [9]

kilometer of a fully loaded VTOL aircraft are stated to be 52% lower than the combustion engine powered car (1.54 seat-load factor), and 6% lower than the battery-powered car (1.54 seat-load factor) with additional benefits in terms of travel time.[6]

Local emissions by UAM, in the city environment, could be almost zero if battery electric propulsion systems are used. Most of the reviewed UAM concepts already rely upon this propulsion type, with a minority working on hybrid electric propulsion systems."[7]

1.2 Concept description

The Mother & Baby Shuttle concept (Figure 1.9) presents a futuristic aerial solution for last mile delivery in suburban areas. This concept is conceived to leverage urban air mobility to alleviate traffic congestion caused by traditional delivery trucks. The Mother & BabyDrones Shuttle consists of a central aerial platform, the Mother Shuttle, equipped with multiple BabyDrones responsible for handling packages.

To address the limitations of long-distance and high-capacity delivery drones,

Figure 1.9: Mother & BabyDrone Shuttle (MbdS)

the solution approach focuses on two key aspects: range and load capacity. A multicopter design is employed for the delivery drone, maximizing its load capacity. To overcome the challenge of limited range, the delivery drone is attached to the bottom of the aircraft, conserving energy during transportation from the warehouse to the vicinity of the consumer's house.

The delivery drones, referred to as the "baby drones" carry packages intended for each individual consumer. Multiple baby drones are then consolidated and placed inside a larger aircraft referred to as the "Mother Shuttle." This integrated system enables efficient movement of packages from the warehouse to the vicinity of the consumer's house.

Upon reaching the designated delivery location, the mother shuttle releases the baby drones from the air, ensuring direct delivery to the consumer's doorstep. After completing the delivery, the baby drones return to the mother shuttle, and together they make their way back to the warehouse. This process ensures smooth delivery operations and prepares the system for subsequent deliveries. To support this delivery system, a new warehouse design, which is going to be introduced in Chapter 2, is required for automate package allocation to the BabyDrones.

By integrating the aerial platform with the delivery process, the Mother & Baby Shuttle offers an extended travel distance capability and higher payload capacity compared to conventional drones.

Chapter 2

Concept Design

In the early stages of industrialization, companies focused on increasing production and output to meet the demands of growing markets. The goal was to produce as much as possible and then push those products into the market, assuming that customers would purchase them. This push system also referred to as "production-driven" or "supply-driven" allowed manufacturers to take advantage of economies of scale and mass production techniques.[10]

However, over time, the focus shifted towards understanding and meeting customer needs more effectively. This change gave rise to a customer-centric approach known as "demand-driven" production.[10] Instead of pushing products into the market, companies began to emphasize understanding customer preferences, tailoring products to meet those preferences, and aligning production with actual customer demand.

When designing a new product, particularly one dedicated to the future , the design thinking process necessitates starting with the identification of customer needs. The introduction of a new product or concept begins by exploring the market's requirements, specifically the pain points experienced by current online shoppers, as well as their future expectations regarding delivery.

This section delves into a description of the Mother&babydrones Shuttle (*MbdS*) solution, elucidating its preliminary design and the driving factors behind its conception. By meticulously examining the choice of the target market, the genesis of the *MbdS* solution is unveiled, followed by an exposition of each module within the system: the shuttle and the drones. These integral components are intricately elucidated in terms of their structural composition and operational modalities, emphasizing their seamless integration within the last mile delivery context.

2.1 Market research

This section justifies the selection of the grocery market and suburban areas as the operational framework and target market for the *MbdS* solution. It presents

the findings of the conducted market research, which aimed to gather insights into the needs and preferences of customers in suburban areas and the challenges associated with last mile delivery in such locations.

The assessment of various markets unveiled the significant potential and challenges within the grocery market. Beyond the general need for faster delivery, the grocery market demands an extra level of care. Handling fresh products necessitates proper storage conditions and swift delivery. In the case of online grocery delivery becoming the predominant method, future users will expect near-instantaneous delivery within a time range of 10-15 minutes.

The presence of issues in this market served as a motivation to develop the *MbdS* solution that could effectively address its most crucial needs. The focal point of the solution lies in meeting the time and quality (freshness) requirements for goods, all while ensuring economic viability in terms of number of orders fulfilled per trip.

Having identified the grocery market as the target market, the exploration commenced to determine the specific group of residents to serve. In this particular instance, the focus was on people residing in suburban areas, commonly known as commuter town[1] residents or "commuters". Suburban residential neighborhoods mainly composed of detached houses and often located far away from city centers, car ownership is often high and public transport is generally less available, which tends to favor the use of private cars[11], to reach nearby stores even for basis food necessities, contributing to higher traffic congestion and emission. Therefore suburban areas has been selected as a potential operational context for MbdS.

Before delving into the solution for the last-mile challenge, it was crucial to gain a comprehensive understanding of the primary beneficiaries and the specific consumer groups that will be predominantly affected by this concept. They are universally classified into 4 types :

1. **Generation Z** : It refers to the generation between the millennials and the alpha generation. Demographers generally classify those born in the mid/late 1990s through the early 2010s as Generation Z. In general, it is classified as a generation that has spent their teenage years since the early 2010s, when smartphones began to spread in earnest.

2. **Millennials** : A generation and population group between Generations X and Z. Demographers classify millennials as people born between the early 1980s and the mid-1990s or early 2000s, especially those born between 1981 and 1996.

3. **Generation X** : Generation X is the generation born in the West after the end of the baby boom after World War II. Although there is no strictly

[1] A commuter town is a populated area that is primarily residential rather than commercial or industrial. Routine travel from home to work and back is called commuting, which is where the term comes from. A commuter town may be called also "bedroom community" or "bedroom suburb" (US)

Shopper Types	Baby Boomer	Gen X	Millennial	AVG US Adult
In Store Regular	77%	70%	65%	68%
Considerers	17%	26%	25%	22%
Interchangers	5%	3%	8%	6%
Online Regulars	1%	1%	2%	2%
Online Deliver to Home	43%	39%	29%	35%
Online Pick up at Store	43%	43%	56%	49%
2017 Online Orders %	12%	24%	43%	10%
2019 Online Orders %	18%	40%	45%	25%

Figure 2.1: Grocery shopper types analysis.
[12]

defined time standard, it usually refers to the years from 1965 to 1980 in the US.

4. **Baby boomers** : The Baby Boom Generation refers to the generation born during the Baby Boom period, usually from 1946 to 1964 after World War II

Comparing the demographic data between where an average US adult lives and what generation they represent helps recognize where new customers might exist for grocery delivery services. The majority of the US population lives in a suburban geography with about half each of the Baby Boomer, Gen X, and Millennial population calling it home.[12]

The Suburban Millennial profile provides details on a large proportion of the US population and that over 40% of them shop online for their groceries. In contrast, Suburban Baby Boomer customer type outnumber millennials population in the suburbs and have more economic resources to try new services.[12]

As they continue to age, preferences could change due to decreases in their mobility and limited access to grocery stores. As of 2018, only 17% of Baby Boomers have used online grocery shopping as compared to 40% of millennials. As a group, they have large growth potential for online shopping. These and other trends from the persona's demographics could be used to create specific groups for focused marketing about delivery service value.

Primary characteristics for the average US adult grocery shopper:[12]

1. They travel seven times a month to the store
2. 70% of them only self-deliver groceries
3. They do the primary shopping for their household
4. All groups use multiple stores to source their groceries

2.2 Ideation Phase

The design process of an Urban Air Mobility (UAM) vehicle entails a thorough examination of various UAM concepts to determine the appropriate configura-

tion of rotors and wings. In particular, the styling architectures of the mother shuttle model were deliberately intended to be innovative. This section presents the team's decisions regarding the distinctive feature of the MotherShuttle (MS) and outlines the relevant literature on which these choices were founded.

Based on the findings from market research and an investigation into commuters' lifestyles, addressing the challenges of last mile delivery necessitated surpassing the limitations posed by delivery drones, such as restrictions on parcel weight and maximum travel distance. This is particularly crucial due to the considerable distance between suburban residents and distribution centers, rendering conventional drones impractical for long-distance deliveries. Moreover, for the solution to be economically feasible, it was essential to design a delivery trip that caters to multiple users.

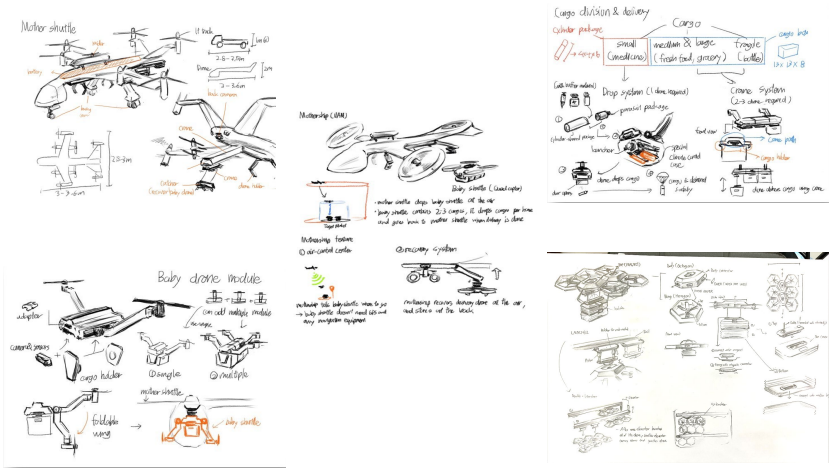

Figure 2.2: MbdS sketching during ideation phase

Throughout the project process, the framework of the *MbdS* remained consistent. However, the external design of both the shuttle and drone modules underwent several modifications.Figure 2.2 shows a collection of the initial flying solution sketching crafted by the team designer.

The final styling model of the main aerial platform responsible for handling the delivery is depicted in Figure 2.3. In this design, a tandem-wing quadplane configuration has been selected for the wing arrangement, drawing inspiration from the "Wingeon" concept in Figure 2.4a [13]. The wings in MotherShuttle solution are equipped with winglets, resulting in the inclusion of four winglets. It is important to note that the utilization of four winglets in a UAM context requires validation, which will be further discussed and examined in Chapter 4.

Regarding the propulsion system, a configuration featuring three tiltrotors has been chosen over the lift and cruise rotor configuration commonly found

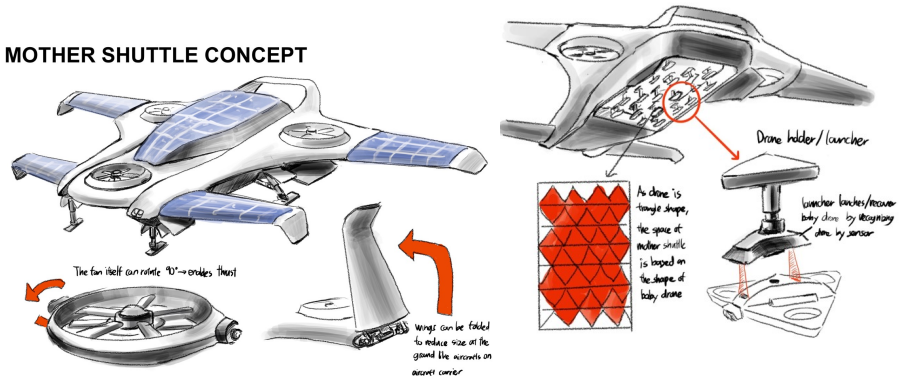

(a) Mother Shuttle External Shape (b) Mother Shuttle Parcel Bay

Figure 2.3: MotherShuttle final styling model

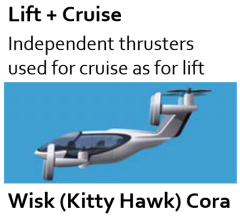

(a) Wigeon concept - tandem-wings [13]

(b) Lift and Cruise configuration [7]

Figure 2.4: Reference Models

in UAM vehicles. This decision was motivated by the advantages offered by tiltrotors, including improved cyclic and collective control. Additionally, the use of three tiltrotors enables three-axis control of the vehicle during vertical flight through the differential adjustment of motor speeds.[14]

2.3 Baby Drones Module

The baby drone module (Figure 2.5) is a compact and lightweight drone measuring approximately 30 centimeters in height. It is designed with a focus on load capacity rather than long-range travel, capable of delivering up to 5 kilograms of cargo. Transported on the mother shuttle, the baby drone is intended for efficient and localized deliveries.

During operation, when the mother shuttle directly passes over the delivery destination, the baby drone is released and rapidly descends. The entire process,

Figure 2.5: Baby Drones Module

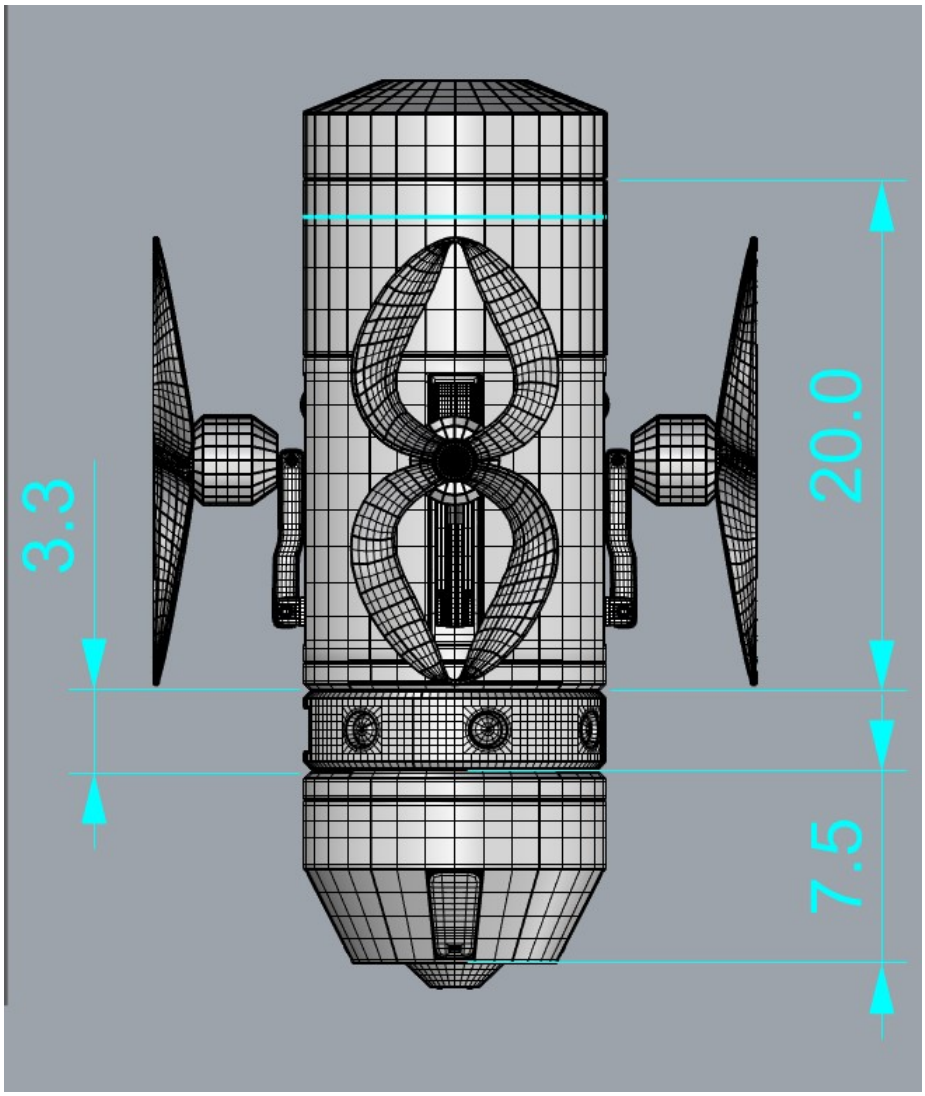

(a) Side view - Folded wings

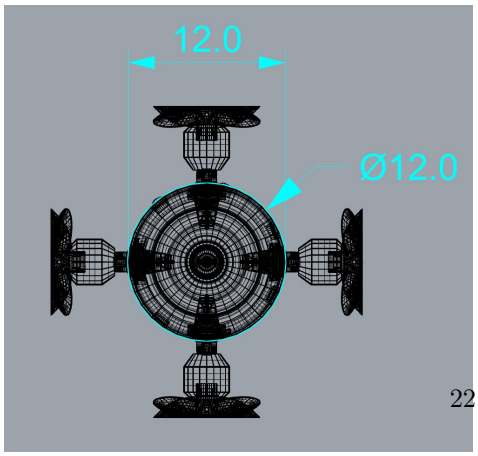

(b) Top view - Folded wings

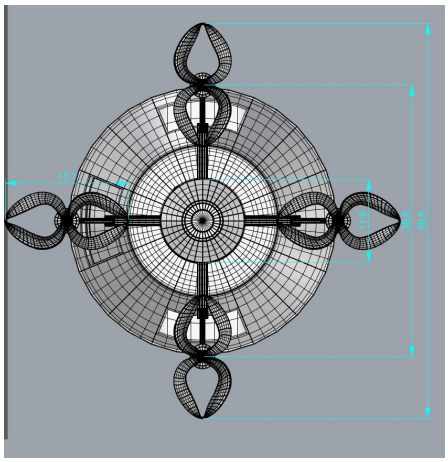

(c) Bottom view - Open wings

Figure 2.6: Baby Drones Dimensions

from detachment to cargo delivery at the customer's doorstep, takes approximately 3 minutes. With a fuselage diameter of 12cm and a package diameter of 19cm, the baby drone is capable of landing in various locations within a space of 400cm^2.

The baby drone's modular design, depicted in Figure 2.7, allows for flexible combinations of modules to suit different situations. Each module, including the body, battery, camera, and cargo adapter, can be combined or customized as needed. For instance, to accommodate cargo exceeding 5kg, two drone bodies can be combined to increase carrying capacity. Similarly, in adverse weather conditions requiring enhanced sensor capabilities, two sensor modules can be combined to improve situational awareness. When combining different modules, the *Adapter* at the bottom of one module is inserted into the top of the desired module, followed by a clockwise rotation of 30 degrees to secure the connection. For instance, in the case of combining two drones for increased load capacity, the adapter at the bottom of one drone is inserted into the top of the other module (*Arresting Module*) of the second drone, and then rotated clockwise by 30 degrees to secure them.

The cargo *Adapter* located at the bottom of the drone features a tapered shape, and when combined with the package, four supporting legs, referred to as *Adapter Locking Legs* in Figure 2.7, extend from the front, rear, left, and right to securely hold the package. During delivery, the four supports retract back into the adapter, releasing the package.

To optimize space utilization within the mother shuttle, the drone's wings can be folded in two stages, reducing the overall surface area. At the top of the drone, an *Arresting Module* combines with the mother shuttle using an electromagnet at the bottom of the *Catcher* to ensure stability during the retrieval process.

Within the mother shuttle's cage, an elevator mechanism is employed to draw the drone inside. Prior to storage, *Wing Protector* device is activated to safeguard the propellers of the drones. A small cylindrical device called the *Catcher*, equipped with electromagnets at the bottom center and concealed Catcher Locking Leg, similar to the *Adapter Locking Legs* in Figure 2.7, securely holds the drone once it is attached to the electromagnet. Upon attachment, the four *Catcher* supports extend to fully secure the drone in place. Subsequently, the drone folds its wings, and the *Catcher* is retracted into the *Shuttle Cage* via a wire connected to the elevator. During this process, the *Wing Protector* descends to shield the drone's propellers. Finally, the elevator ascends inside the *Shuttle Cage*, safely storing the drone system within the mother shuttle. To release a drone, the process is reversed.

The package specification utilized in the MbdS solution is illustrated in Figure 2.8. In contrast to conventional packages, the new cargo package introduced in this concept is made from durable plastic material and designed to be reusable. This eliminates the reliance on fragile packages that are difficult to recover and contribute to waste generation.

Furthermore, the cargo package includes a top cover that allows for seamless

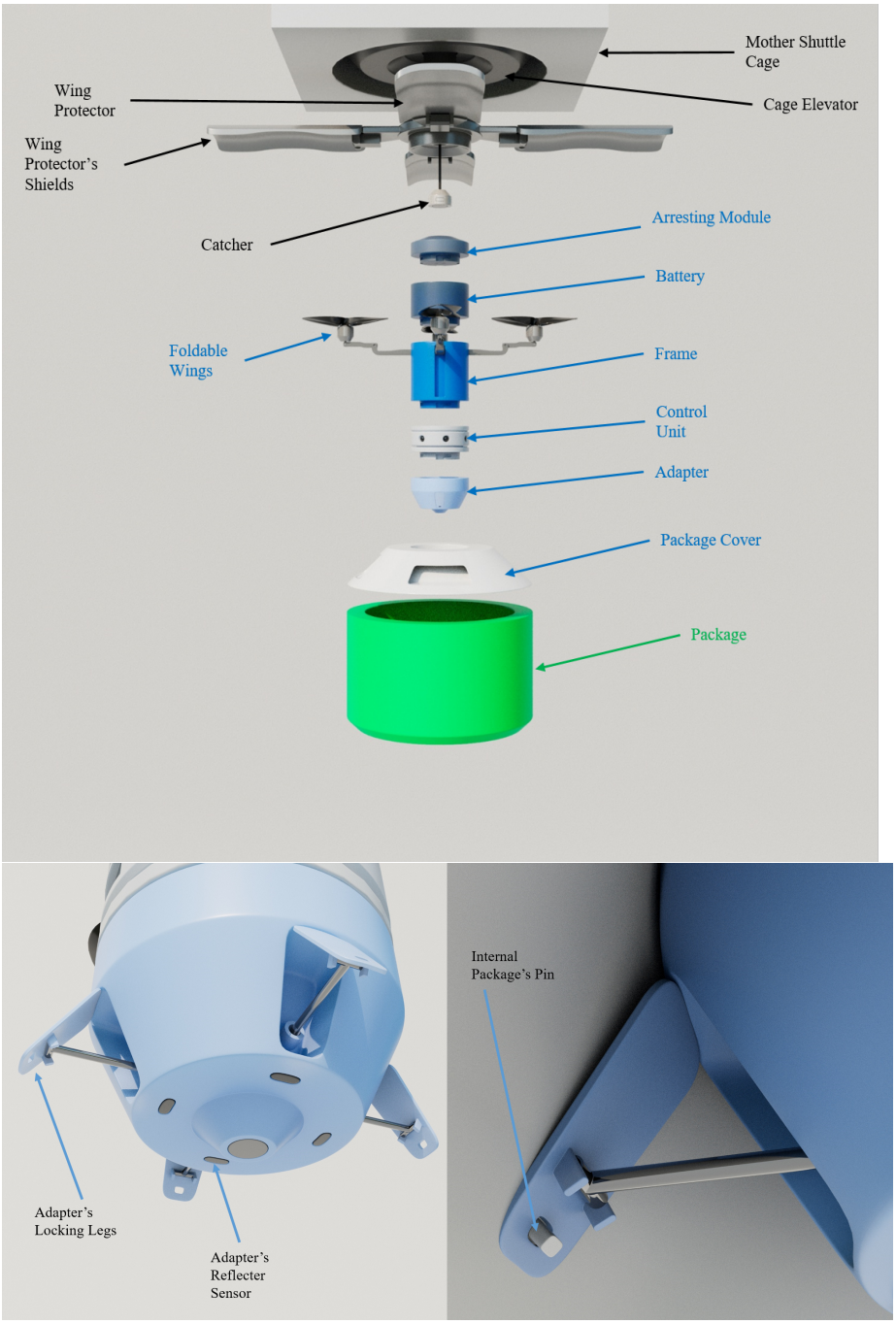

Figure 2.7: Baby Drones modular structure

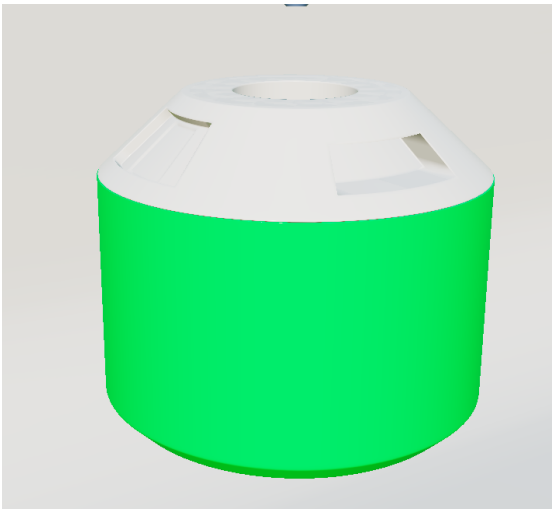

Figure 2.8: Baby Drones' package spec

integration with the baby drone module using the previously mentioned *Adapter* and equipped with side handles to facilitate easy removal

2.4 Mother Shuttle Module

The Mother Shuttle, measuring 6 meters in length, is defined as an Urban Air Mobility (UAM) vehicle designed to accommodate up to 32 baby drones and 32 cargoes simultaneously. The Mother Shuttle compensates for the reduced range of the baby drone by prioritizing load capacity, thereby enabling long-distance deliveries that were previously unattainable with conventional drones.

Powered by electric propulsion, the Mother Shuttle incorporates a large battery positioned atop the aircraft and utilizes solar panels on the wing surface to enhance energy efficiency. To address the thermal management concerns of the battery, an air duct is placed in front of it, facilitating the inflow of air and coupling it with cooling water.

In terms of aerodynamics, the Mother Shuttle features canard wings and utilizes engine vectoring instead of a single vertical tail. This configuration allows for easy storage in logistics warehouses, eliminating height restrictions associated with vertical tails, and enhances stability by preventing stall through the use of canard wings. Additionally, both wings are equipped with winglets, effectively reducing vortices and enhancing overall aerodynamic performance, specifically the lift as it will be elaborated in Chapter 4.

In aircraft design, a canard refers to a smaller wing positioned near the front of the aircraft, ahead of the main wing. It operates at a higher angle of attack compared to the main wing, generating lift and contributing to the overall lift of the aircraft. By maintaining a balanced distribution of lift along the wingspan,

Drones Specifications	Description
Net weight	3 Kg
Total Loaded Weight	8 Kg
Propeller	**GF6042**
Diameter	152.4 mm
Motor (x4)	**SmooX 2806 1750KV**
Load Current	35 A
Voltage	21 V
Power	735 W
Battery	**Foxtech 22.2V 6S 16000mAh Li-ion Battery**
Weight	1.5kg
ESC (Electronic Speed Controller)	Simon 40A-UBEC
Image sensor	DSJ-3808-308
LIDAR	RPLIDAR A1
GPS(Gyroscope)	ATGM336H-5N

Table 2.1: BabyDrones Technical Specifications

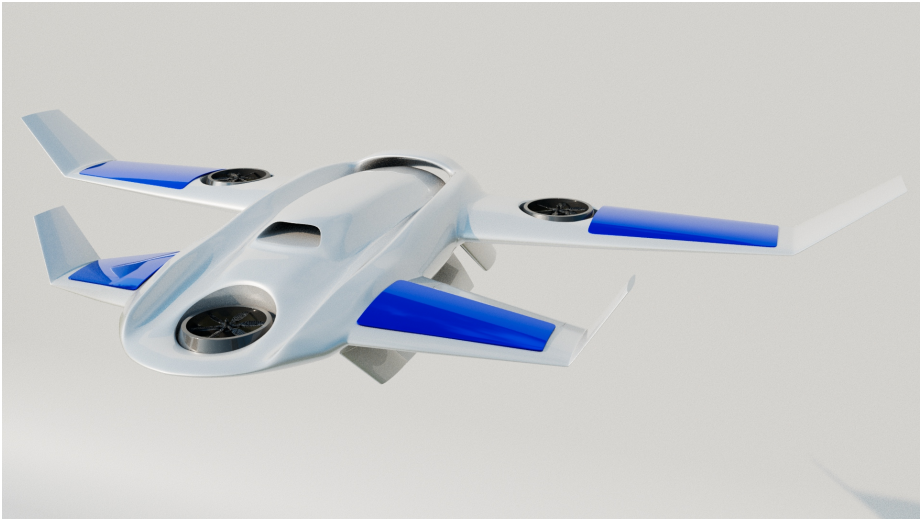

Figure 2.9: Mother Shuttle aircraft

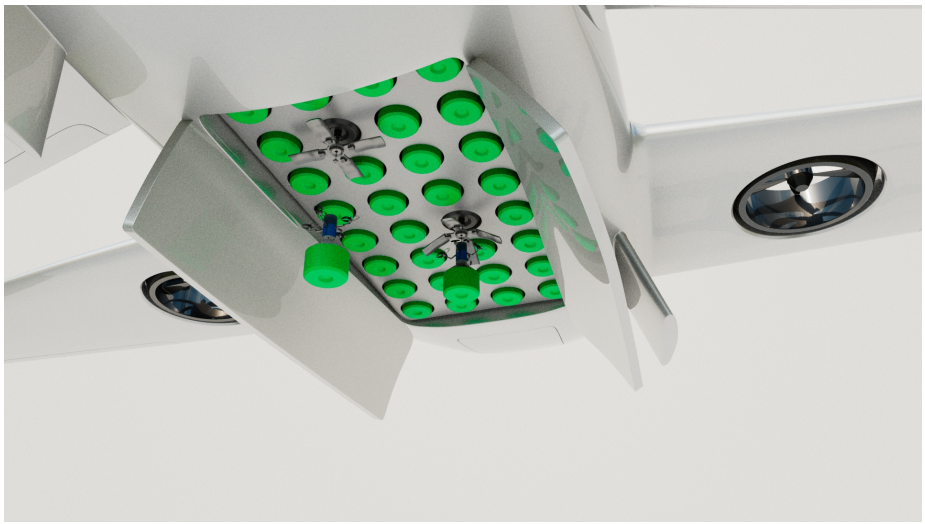

Figure 2.10: Mother Shuttle Bay

the canard wing allows the main wing to operate at a lower angle of attack, thereby delaying stall and improving aerodynamic stability.

The propulsion system of the aircraft relies on three duct fans, which can be angled up to 90 degrees to enable vertical take-off and landing (VTOL). During takeoff and landing, the duct fans align horizontally with the wings, while during flight, they are oriented vertically to generate forward momentum. The rear wing rotors primarily generate lift, while the central duct fan is responsible for center thrust. The thrust-adjustable duct fan on the main wing controls the rotation of the vertical axis, effectively replacing the need for a vertical tail.

To minimize drag during flight, the landing gear at the bottom of the aircraft is designed in a wing-like shape. The center of the shuttle houses the cargo compartment referred to as the "shuttle bay". Typically covered to shield it from external temperatures, the bay opens only when the Mother Shuttle reaches the delivery location, allowing for the release of the baby drones as it hovers over the designated area.

UAM Shuttle Specifications	Description
Empty Weight	1963 kg
Weight at Take-off	2475 kg
Propeller Diameter	2.134 m
Power Required Per Propeller	360 kW
EMRAX 348 Motor Peak Power (x3)	400kW
Battery	Tesla 4680 Battery Cell

Table 2.2: Mother Shuttle Specifications

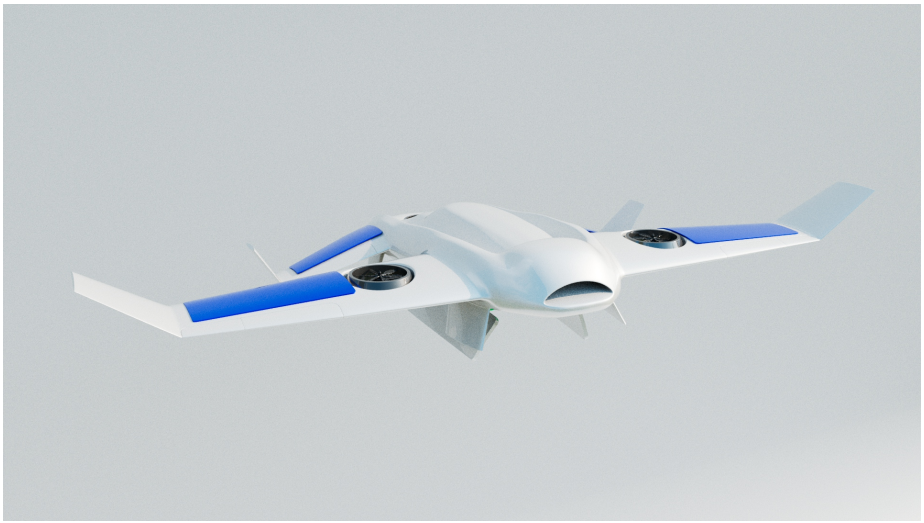

Figure 2.11: Mother Shuttle's rear wings rotors

2.5 Warehouse Planning

To accommodate the aerial delivery solution that connects the warehouse with the end-user, a new warehouse design is introduced in this section. The implementation of the *MbdS* solution requires a warehouse environment that seamlessly integrates the proposed aerial delivery module and optimizes operational efficiency.

The warehouse is structured into three levels, with an additional underground level dedicated to controlled storage(Figure 2.13). Picking robots navigate through a grid system on the underground level, transporting goods from the shelves to the elevator for transfer to the ground floor. The ground floor serves as the packaging area, and potentially for recycling, where goods are prepared and allocated to the baby drones located on the first floor. The first floor acts as the drones' workshop zone, where the "shuttle cage" is loaded with drones before being transported upward through dedicated vertical channels and installed in the respective "shuttle bay." The second floor houses the VTOL platform, serving as the takeoff and landing area once the "shuttle cage" is installed in mother shuttle. This floor represents the final step before the aerial cargo vehicle is ready for delivery. A story-board of the warehouse operations is depicted in Figure 2.12

The vertical flow of materials is achieved by elevators that connect the underground storage to the top floor, enabling the allocation of goods to the aerial cargo vehicle. Another set of elevators facilitates the transition between the first

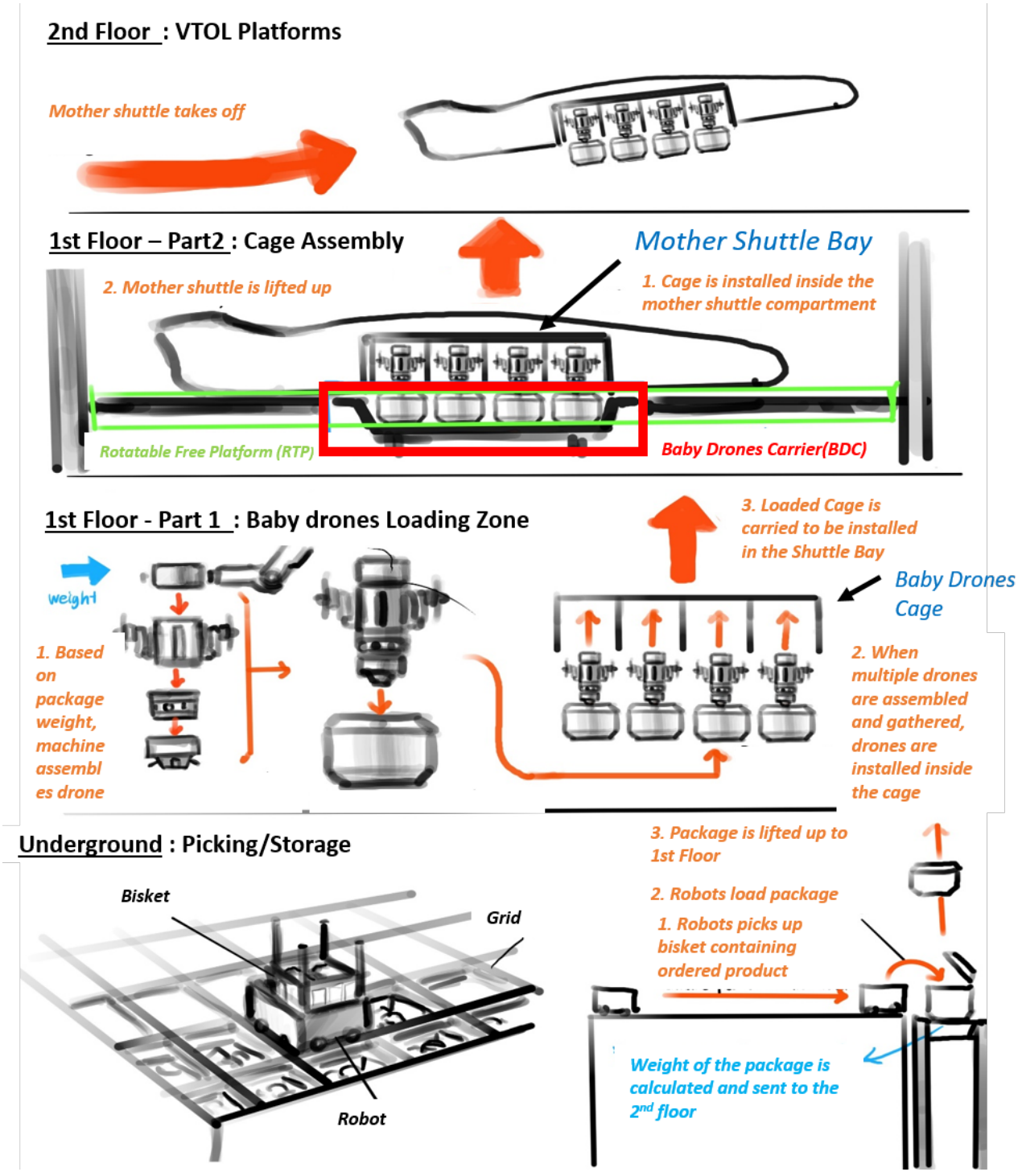

Figure 2.12: Warehouse operation story board

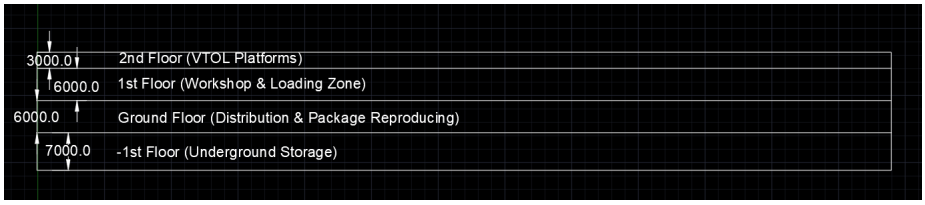

Figure 2.13: Floors Deployment

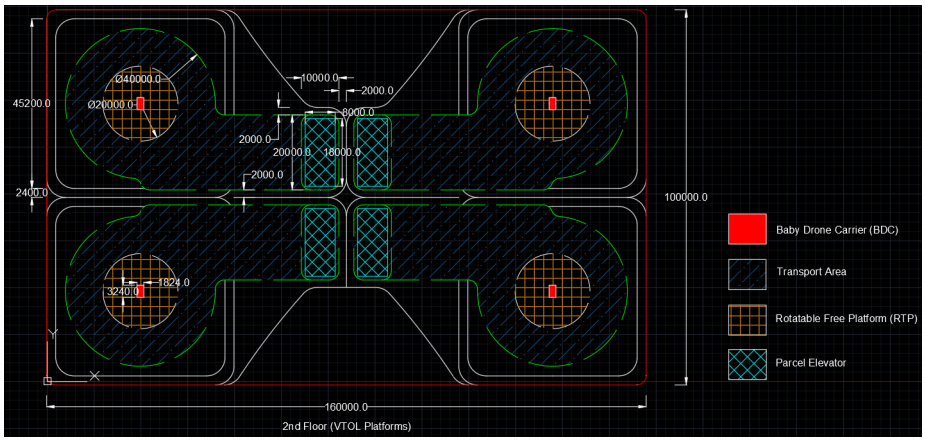

Figure 2.14: Warehouse 2nd floor plan - VTOL platforms

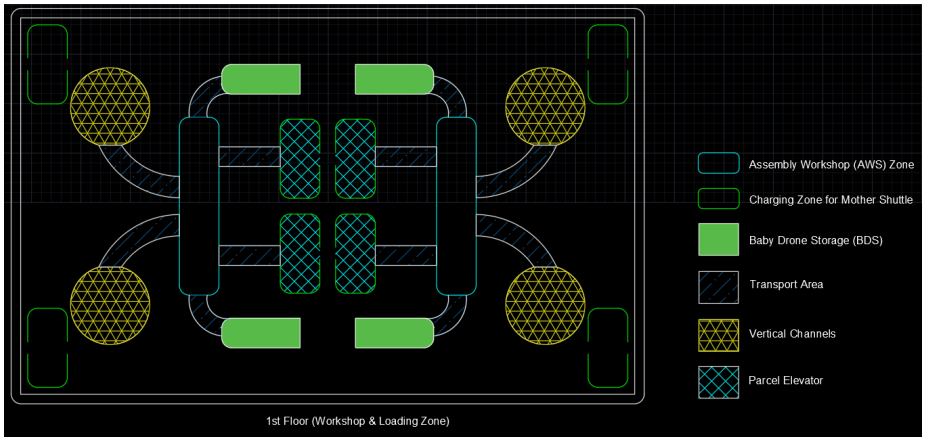

Figure 2.15: Warehouse 1st floor layout - Workshop and loading zone

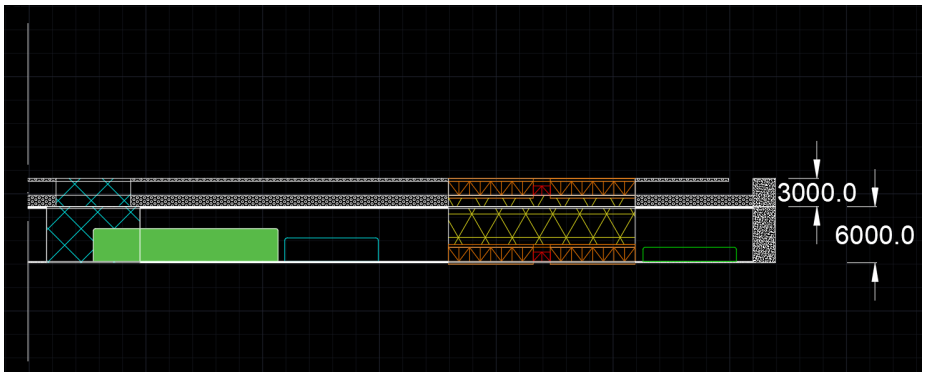

Figure 2.16: Warehouse 1st and 2nd floor side view section

and second floors, linking the drones' workshop zone to the dedicated shuttle platform. Additionally, to enable packages recycling operation in future distribution centers, dedicated downward vertical channels are implemented, starting from the top floor VTOL platform and ending on the ground floor where recycling occurs in the same floor where packaging is being fulfilled.

The Baby Drones Carrier**(BDC)**, labeled in Figure 2.14 serves as a dedicated transporter for the "shuttle cage" between the second and first floors, as previously mentioned and depicted also Figures 2.15 showing first floor layout.

The carrier is responsible for transporting the "shuttle cage" which contains the drones loaded with delivery packages, from the baby drones' assembly workshop zone on the first floor Figure 2.15 to be installed in the shuttle bay of the cargo vehicle located on the rooftop. Similarly, it is used to unload the "shuttle cage" from the shuttle bay after landing on the Rotatable Free Platform **(RTP)** in the rooftop and return it to the baby drones' workshop zone. The **BDC** is integrated with the platform **(RTP)** so that the installation of the "shuttle cage" to the "shuttle bay" can occur seamlessly in the first floor.

The Rotatable Free Platform **(RTP)** (Figure 2.14) serves as the actual take-off and landing platform for the mother shuttle. It allows for the installation of the "shuttle cage" and is rotatable to enable the shuttle to fly in any direction for delivery. The **RTP** platforms can also move downward to the first floor through the downward vertical channels. This enables the charging operations and the installation of the shuttle cage in the "shuttle bay". The downward platform channel, present in all the warehouse floor plans, allows for the downward flow of empty packages retrieved from the shuttle cage on the rooftop, facilitating recycling operations on the ground floor(Figure 2.17)

The first floor plan, shown in Figure 2.15, is where the allocation of packages to the baby drones and the assembly of the drone system in the "shuttle cage" take place. Packages from the ground floor are transported via the elevator located in the middle, and the baby drones from the "storage zone for baby

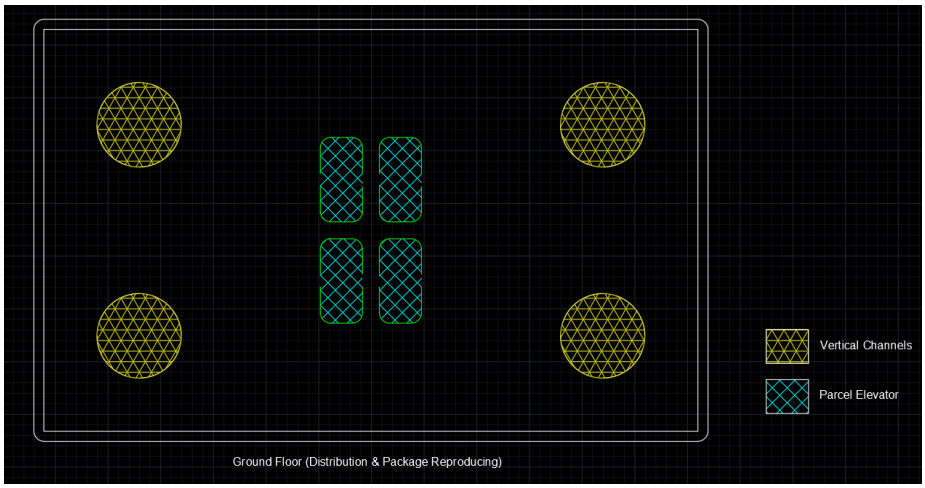

Figure 2.17: Ground floor layout - Packaging & future recycling area

drones" are assembled in the "Assembly Workshop" on the first floor. Once the shuttle cage is filled with loaded drones, the **BDC** transports it to its designated spot in the middle of the **RTP** platform. Once in place, the shuttle cage is installed in the shuttle bay, and the **RTP** platform can be raised to the top floor, allowing the cargo shuttle to embark on its delivery mission.

Figure 3 depicts the floor plan of the underground storage area, where packages are stored. The central vertical elevator facilitates the transportation of packages within the warehouse.

A final rendering showing the external building shape of the above described future warehouse is presented in Figure 2.19. Summarizing the main new units introduced in the warehouse hosting the MbdS solution:

1. **Assembly Workshop (AWS) Zone** - *1st floor*: This unit serves as the area where the baby drones and packages are assembled and mounted in the shuttle cage.

2. **Rotatable Free Platform (RTP)** - *1st/2nd floor*: The RTP is a VTOL platform that can move between the first and second floors. It integrates the Baby Drone Carrier (BDC) and serves as the assembly point in the 1st floor and as a VTOL platform in the 2nd floor, allowing flexibility in the direction of takeoff.

3. **Baby Drone Carrier (BDC)** - *1st floor*: The BDC is responsible for transporting the shuttle cage from the AWS to the RTP platform, where it is installed inside the mother shuttle body.

4. **Baby Drone Storage (BDS)** - *1st floor*: This unit is dedicated to store the baby drones that will be loaded and installed in the shuttle cage in

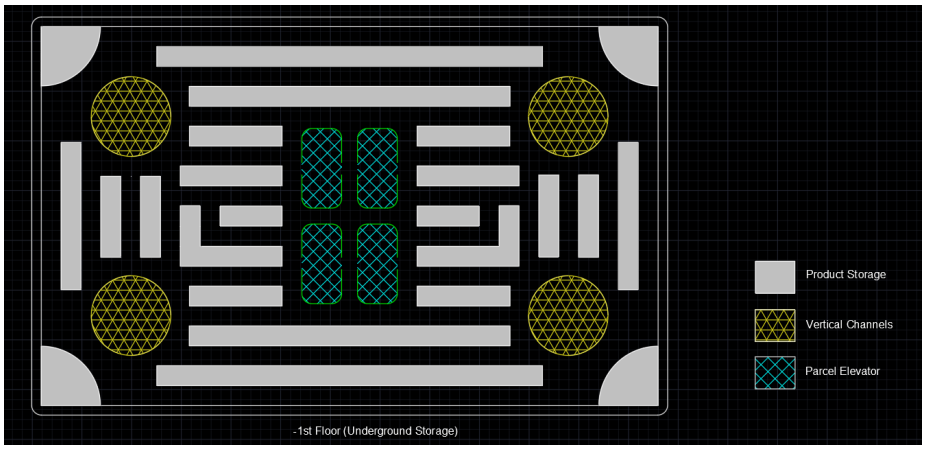

Figure 2.18: Warehouse Underground storage layout

the AWS.

5. **Parcel Elevator** - *All floors*: The parcel elevator, located in the middle of the warehouse, facilitates the vertical transport of packages between different floors.

6. **Vertical Channels** - *All floors*: These vertical channels, located in the corners of the warehouse, serve multiple functions. They enable the movement of empty packages from the top floor to the ground floor for recycling purposes and also allow for the elevation and lowering of the RTP platform.

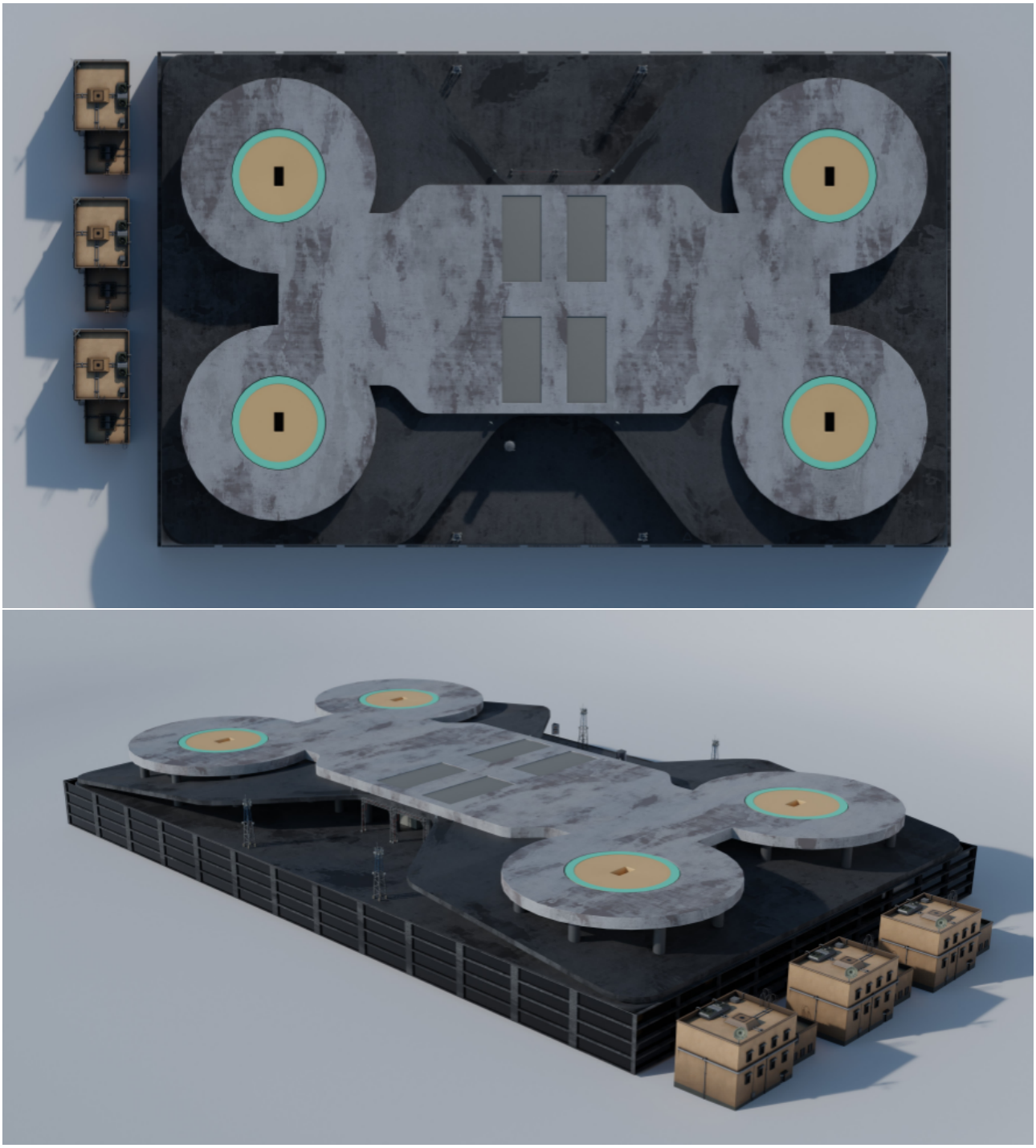

Figure 2.19: MbdS Warehouse Building

Chapter 3

CFD Fundamentals & Simulation Set-Up

This chapter provides an overview of the simulation parameters and the fundamental theory behind Computational Fluid Dynamics field. The theoretical discussion that follows have been expanded upon in [15] The geometry of the model and the selected winglet configurations are introduced and the simulation parameters and meshing are specified. Boundary conditions are discussed to ensure the appropriate selection of control variables.The last section explains the turbulence modeling approach employed in the simulation of the case study aircraft.

The simulation conducted in this thesis aims to answer the question of the benefits associated with the winglet device. The objective is to determine whether it is still advantageous to add such a device to each wing of the described cargo vehicle, resulting in 4 winglets aircraft. Chapter 4 will delve into the details of this investigation and its findings.

3.1 Governing Equations of Fluid Motion

Considering a steady laminar flow in a viscous, incompressible, Newtonian fluid without free-surface effects. The governing equation of fluid motions are Equation 3.1 that ensures the preservation of mass within a fluid system and Equation 3.2 which represents the transport equation for linear momentum.

In the simulation, turbulent flow is considered to replicate realistic flying conditions. The incorporation of turbulent flow necessitates turbulence modeling, which will be discussed in Section 3.5.

1. Continuity Equation

$$\overrightarrow{\nabla} \cdot \overrightarrow{V} = 0 \tag{3.1}$$

2. Navier-Stokes Equation

$$(\overrightarrow{V} \cdot \overrightarrow{\nabla}) \cdot \overrightarrow{V} = -\frac{1}{\rho}\overrightarrow{\nabla} P' + \nu \nabla^2 \overrightarrow{V} \tag{3.2}$$

Where :

- $\overrightarrow{V}$ is the fluid velocity vector. In the Cartesian form, $\vec{V} = u\hat{i} + v\hat{j} + w\hat{k}$
- ρ fluid density
- ν kinematic viscosity
- P' is the *modified pressure* neglecting the gravity term in Navier-Stokes equation.

In flows without free-surface effects, gravity does not significantly impact the dynamics of the flow. Its primary influence is to superpose a hydro-static pressure on the dynamic pressure field. Gravity becomes important in flows with free surfaces, such as waves, ship motion, or spillways from hydroelectric dams. However, in engineering problems where there is no free surface, such as pipe flow, submerged flow around a submarine, or the motion of vehicles and aircraft, the effect of gravity on flow dynamics is limited to a hydro-static pressure distribution in the vertical direction. This hydro-static pressure is combined with the pressure field generated by the fluid flow. In essence, gravity's role is absorbed by the pressure term P' in the equation. It is worth noting that for incompressible flow, density and viscosity are constant terms in the equations of fluid motions.

3.2 Input Model

In order to test the effect of the winglet on the mother shuttle aerodynamic performance, a baseline model shown in Figure 3.1 have been imported to Star-CCM+ environment with the dimensions presented in table 3.1. Then 3 different winglet configurations, displayed in Figure 3.2 have been created and added later to the tip chord of the front and rear wings.

The mother shuttle concept is a VTOL (Vertical Takeoff and Landing) aircraft that undergoes various flight phases (Figure 3.3), each characterized by unique aerodynamic conditions. To capture the transient phenomena associated with these flight phases, an unsteady simulation approach has been employed.

Unsteady simulations enable the examination of time-dependent flow phenomena, such as vortex shedding and flow separation. These phenomena have a significant impact on the aerodynamic performance of the aircraft, influencing its stability and control. The turbulence viscosity ratio, specified in Table 3.2 represents the ratio of the turbulent viscosity to the molecular viscosity in the fluid flow simulation. It influences the behavior and accuracy of the turbulence model used in the CFD simulation. In general, a turbulence viscosity ratio

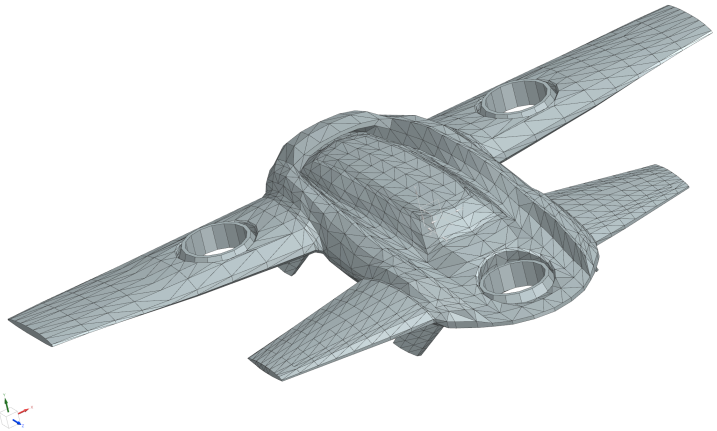

Figure 3.1: Mother shuttle CFD Baseline Model

Geometry	Value
Total Length (m)	6.14
Front Wings Span b_1 (m)	9.97
Rear Wings Span b_2 (m)	6.1
Root Chord (Front and Rear) c_r (m)	2.2
Front Wings Taper Ratio λ_1	0.45
Rear Wings Taper Ratio λ_2	0.54
Frontal Area A (m^2)	5.2
Total Wings Area W (m^2)	17.28

Table 3.1: Mother Shuttle CFD Model Specifications

of unity indicates that the turbulent viscosity is equivalent to the molecular viscosity, implying a fully turbulent flow. A value higher than one represents enhanced turbulence, while a value lower than one indicates reduced turbulence.

In this study, the focus was specifically on the cruising flight condition of the mother shuttle. As an eVTOL aircraft designed for cargo transport, it can reach speeds of up to 180 km/h during cruising. The decision to simulate this flight condition was motivated by the interest in assessing the effect of incorporating a winglet on cruising performance. Winglets are primarily intended to reduce vortex generation and turbulence in normal aircraft during cruising. Therefore, exploring the impact of winglet integration during other flight conditions was not within the scope of this study.

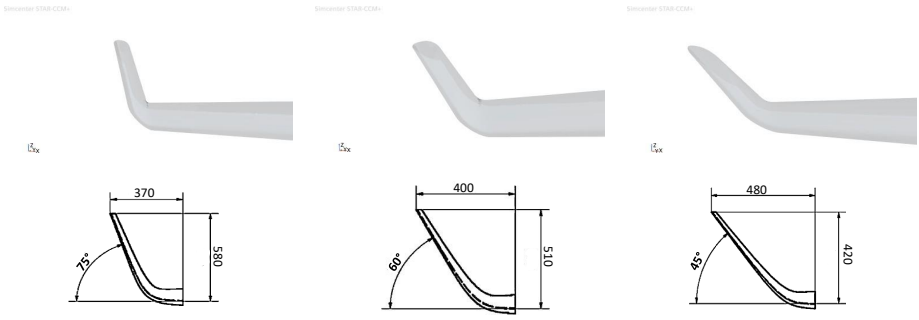

(a) Cant Angle = 75° (b) Cant Angle = 60° (c) Cant Angle = 45°

Figure 3.2: Winglet Configurations Simulated

Properties	Value
Air Density	1.18415 kg/m^3
Air Dynamic Viscosity	$1.85508 \cdot 10^{-5}$ Pa^{-s}
Flow velocity	180 Km/h ($+y$ direction)
Flight Condition	Cruising
Reynolds Number	$2 \cdot 10^7$
Turbulence Viscosity Ratio	10
Flow Behavior	Unsteady
Time step	0.005 s
Iterations	3000

Table 3.2: Simulation Parameters

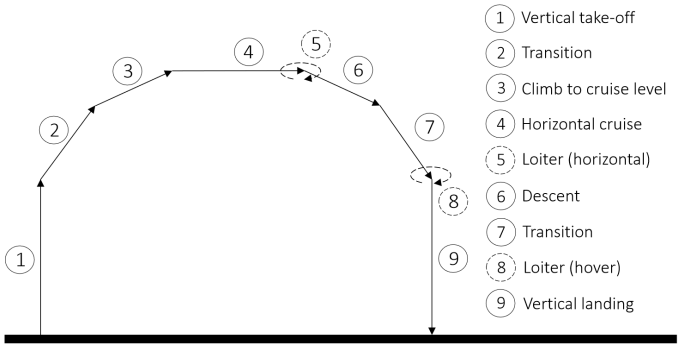

Figure 3.3: 9 flight phases of a regular eVTOL flight mission [13]

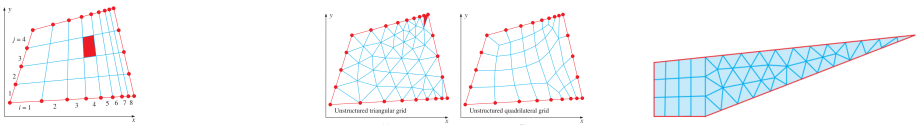

(a) Structured Grid (b) Unstructured Grid (c) Hybrid Grid

Figure 3.4: Different Cell Types
[15]

3.3 Meshing

In computational fluid dynamics (CFD), after defining the computational domain, the Navier-Stokes equations are solved iteratively on a grid composed of small cells. In CFD environment meshing is defined as the process of dividing the domain into these cells. Two main types of grids are commonly used: structured and unstructured grids.

Structured grids consist of planar cells, while unstructured grids feature cells with varying shapes, such as triangles, quadrilaterals, tetrahedrons, or hexahedrons.(Figure 3.4)
For complex geometries, unstructured grids are preferred due to their flexibility in grid generation. In some situations, a hybrid grid approach is adopted, which combines structured and unstructured grids to achieve high resolution near the solid surfaces or boundaries while maintaining coarser grids away from these regions.

In boundary layer, the flow variables such as velocity and pressure experience changes rapidly normal to the wall, leading to high gradients. To accurately capture these flow characteristics, an anisotropic mesh with a prism layer is employed in CFD to resolve boundary layer regions.
Prism layers,so-called because of the method of projecting the mesh faces from the core mesh onto the solid boundary resulting in prism shaped cells, are thin layers of cells that are stacked adjacent to the solid regions of the geometry. They have a triangular or quadrilateral base and are extruded in the normal direction to form a three-dimensional layer.The mesh parameters for the prism layer, including the number of layers (N), total thickness (t), and stretching factor (s) between subsequent layers, are defined in Table 3.3

The generated grid of the mother shuttle, shown in Figure 3.5 consists of a hybrid structure, combining both structured and unstructured cells.

Inspecting the generated mesh, all cells exhibit skewness angles below 85°(Figure 3.7), which falls within the acceptable range. This indicates that the mesh quality is satisfactory and meets the required criteria for accurate (CFD) simulations.

Skewness is defined as the departure from symmetry. Individual cell must not be highly skewed otherwise this can lead to convergence difficulties and inaccuracies in the numerical solution.[15] Speaking about skewness is generally refered to the 2-D **equiangle skewness** with the formula shown in Equation 3.3

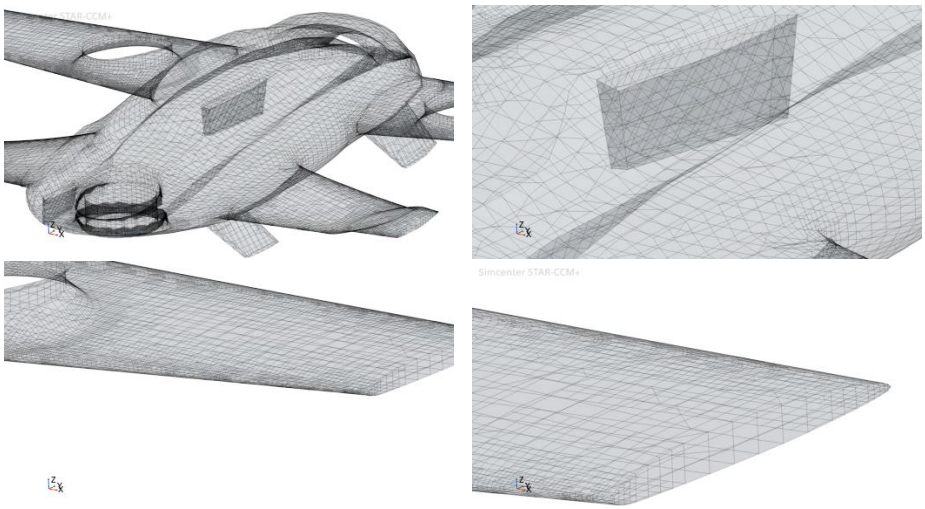

Figure 3.5: Mother Shuttle Grid Generation

(a) Triangular Cells (b) Quadrilateral Cells

Figure 3.6: Skewness
[15]

:

$$Q_{EAS} = \max\left(\frac{\Theta_{max} - \Theta_{equal}}{180° - \Theta_{equal}}, \frac{\Theta_{equal} - \Theta_{min}}{\Theta_{equal}}\right) \tag{3.3}$$

Where:

- Θ_{min} and Θ_{max} : Minimum and maximum angle between any two edges of the cell.
- Θ_{equal}: Angle between any two edges of an ideal equilateral cell with the same number of edges.

For triangular cell $\Theta_{equal} = 60°$ and for quadrilateral cells $\Theta_{equal} = 90°$. Therefore, an equilateral triangle has zero skewness. In the same way, a square or rectangle has zero skewness. Equiangle skewness have a value between 0 and 1 for any 2-D cell.

Meshing Parameters	Value
Cell Base Size	0.1 m
Number of Cells	$2 \cdot 10^6$
Target surface Size	100 %
Minimum Surface Size	10 %
Surface Curvature	36 $Points/Circle$
Surface Growth rate	1.3
Surface Proximity	2 $Points/Gap$
Prism Layer Settings	Value
Number of layers N	2
Prism Layer Stretching factor S	1.5
Prism Layer Total Thickness t	33.33%

Table 3.3: Mother Shuttle Model Meshing & Prism Layer Set-Up

3.3.1 Residual Check

In the numerical solution of the discretized equations, an iterative method is employed. To assess the convergence and solution accuracy, a residual check is performed at each iteration. Residuals represent the error between the computed and exact solutions for each equation in the system. The goal is to achieve convergence, where the residuals stabilize and approach a predetermined value. Ideally, the residuals should reach a lower value, typically in the range of 10^{-4} to 10^{-5}, indicating a more reliable solution. By monitoring the convergence of residuals, the accuracy of the numerical solution can be evaluated.

Figure 3.8 depicts the values of the residuals obtained during the simulation of the mother shuttle model at two different iterations.

3.4 Boundary Conditions

While the equations of motion, the computational domain, and even the grid may be the same for two CFD calculations, the type of flow that is modeled is determined by the imposed boundary conditions. Appropriate boundary conditions are required in order to obtain an accurate CFD solution.

Wall Boundary Conditions

The simplest boundary condition is that of a wall. Since a fluid cannot pass through a wall, the normal component of velocity is set to zero relative to the wall along a face on which the wall boundary condition is prescribed. In addition, because of the no-slip condition, the tangential component of velocity at a stationary wall is set to zero.

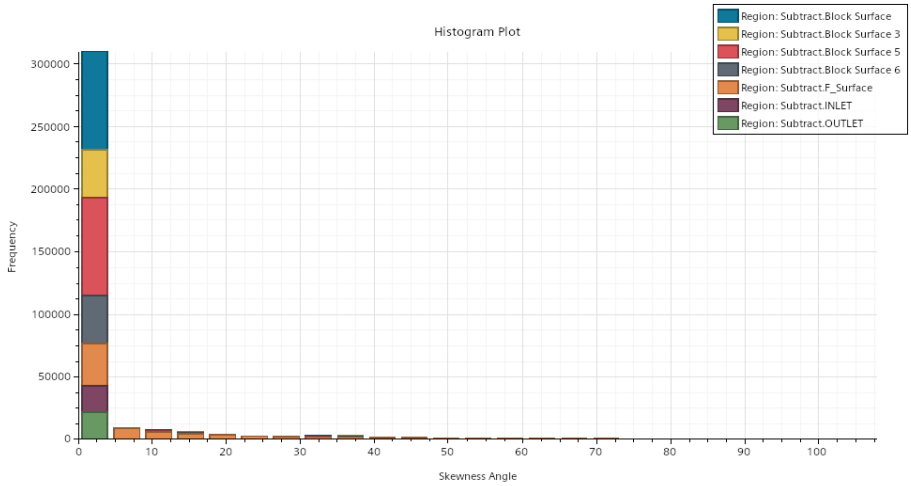

Figure 3.7: Skewness Angle Check

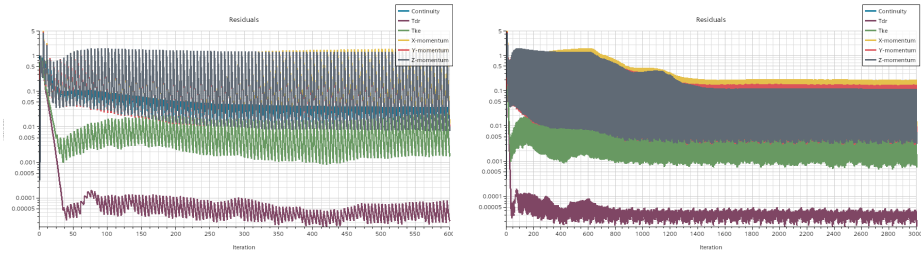

(a) 600 Iterations

(b) 3000 Iterations

Figure 3.8: Residuals

The same can be considered for **symmetry wall**, that is used to enable modelling a portion of the physical flow domain, conserving computer resources and reducing simulation time. The symmetry boundary condition forces flow field variables to be mirror-imaged across the symmetry plane. Mathematically, gradients of most flow field variables in the direction normal to the symmetry plane are set to zero across the plane of symmetry, although some variables are specified as even functions and some as odd functions across a symmetry boundary condition.

Inflow - Outflow Boundary Conditions

There are several options at the boundaries through which fluid enters the computational domain (inflow) or leaves the domain (outflow). They are generally categorized as either **velocity-specified conditions** or **pressure-specified conditions**.

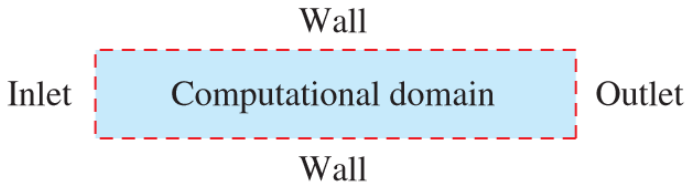

Figure 3.9: Boundary conditions
[15]

At a velocity inlet the incoming flow velocity along the inlet face is specified. At a pressure inlet, the total pressure from the far field where the ambient pressure is known is specified along the inlet face.

At a velocity inlet, pressure is not specified directly to avoid mathematical over-specification, as pressure and velocity are coupled in the equations of motion. Similarly, at a pressure inlet or outlet, velocity is not explicitly specified for the same reason. The values of pressure and velocity adjust themselves at these boundaries to be consistent with the surrounding flow field.

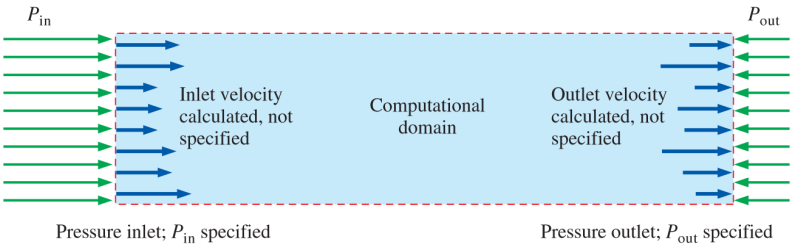

Figure 3.10: Pressure Inlet -Pressure Outlet Boundary Conditions
[15]

At a pressure outlet, where fluid flows out of the computational domain, the static pressure along the outlet face is specified, often set to atmospheric pressure. In the case of turbulent flow simulations, additional turbulent flow properties such as the k-ϵ turbulent viscosity are also specified at pressure inlets and outlets.

3.5 Turbulence Modelling

At larger Reynolds numbers, the fluid's inertia overcomes the viscous stresses, and the laminar motion becomes unstable. Rapid velocity and pressure fluc-

tuations appear and the motion becomes inherently three dimensional and unsteady. When this occurs, this motion is described as being turbulent. [16]

Turbulent flows are unsteady by nature with the presence of continuous fluctuations of velocity, which can produce fluctuations in other scalars as temperature, density and mixture composition. These fluctuations are generated by the presence of vortices (called also eddies) with different scales (sizes) in the flow.

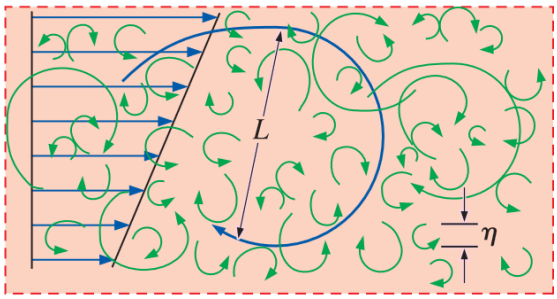

Figure 3.11: Turbulent eddies
[15]

As shown in the figure 3.11, turbulent eddies have various length scale, that is known in the literature with *Turbulence Length Scale*, that is a physical quantity describing the size of the eddies in a turbulent flow. These finer features of the turbulent flow are characterized by being unsteady, three-dimensional, swirling, vortical(rotating around an axis).
The largest eddy size is L and the smallest eddy size is η known as *Kolmogrov Length Scale*. Kolmogrov in 1941 introduced the concept on the energy cascade, that states that the eddies with various length scale (large and small) produce different amount of kinetic energy. This kinetic energy is produced first by the largest scale eddies (size L) that interacts and extract energy from the mean flow. The energy is transferred to the smaller eddies in a rate equal to the *dissipation rate* ϵ, then dissipated by the small eddies (size η), known as *Kolmogrov length scale*, in the form of heat due to viscosity effect of the fluid.
This process is know as the ***Energy Cascade*** process that was also explained by Richardson in 1922 with the following verse[17] :

> *"Big whorls have little whorls,*
> *Which feed on their velocity,*
> *And little whorls have lesser whorls,*
> *And so on to viscosity."*

The contribution of different scales on the turbulent kinetic energy can be defined by the energy spectrum shown in Figure3.13. The spectrum can be divided in three phases :

1. *Energy Production Phase* (Mean Flow energy), which contains the largest eddy scales and concentration of turbulent kinetic energy.

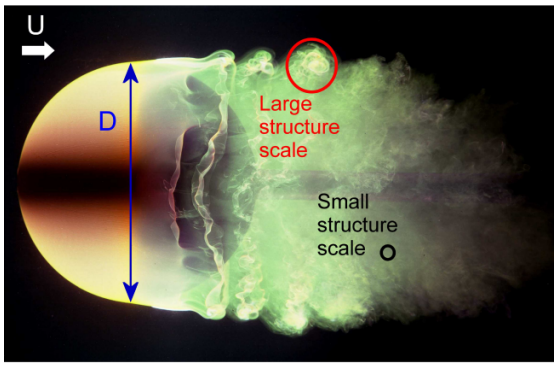

Figure 3.12: Turbulent flow around a sphere

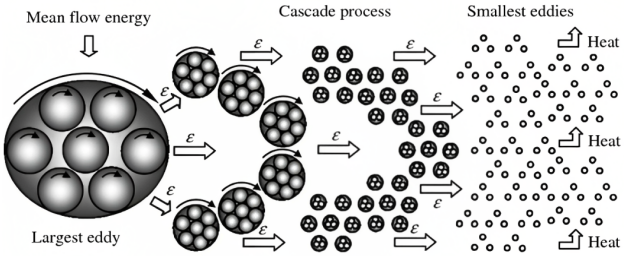

Figure 3.13: Energy cascade in a turbulent flow

2. *Energy Transfer Phase* (Cascade Process), the energy is being dissipated here from the large to smaller eddies in a dissipate rate ϵ equal to the kinetic energy production rate at the large eddies level.

3. *Dissipation of Energy* (Smallest Eddies), the kinetic energy continue to transfer from the largest to the smallest eddies, and at this level the kinetic energy is dissipated into heat. This phase in controlled by the viscosity ν and the dissipation rate ϵ .

Where :

- Kolmogrov Length Scale :

$$\eta = \left(\frac{\nu^3}{\epsilon}\right)^{\frac{1}{4}} \tag{3.4}$$

  ν is the fluid kinematic viscosity and ϵ is energy dissipation rate

- Dissipation Rate :

$$\epsilon = \frac{k^3}{L} \tag{3.5}$$

k is Kinetic Energy extracted from the mean flow by vortex stretching (due to mean velocity gradients)

- Relation between Large and small eddies

$$\frac{L}{\eta} = (Re)^{\frac{3}{4}} \tag{3.6}$$

To simulate turbulent flows with CFD, the different length scales need to be resolved or modeled. An eddy can be resolved if the mesh size used for the simulation is smaller than the size of the eddy. If not, a model needs to be applied to describe the turbulence. Three different approaches for turbulence modeling are distinguished.

1. **Direct Numerical Simulation (DNS)** : In DNS, all the scales involved in the turbulent spectrum are resolved. This implies the solution of the full instantaneous Navier-Stokes equations without any turbulence model. The problem of using this approach is the requirement of high computational resources. As the smallest scales (the Kolgomorov scales)should be resolved considering at least 2 cells. DNS solutions require extremely fine, fully three-dimensional grids, large computers, and an enormous amount of CPU time. [18]

2. **Large Eddy Simulation (LES)** : With this technique, large unsteady features of the turbulent eddies are resolved, while small-scale dissipative turbulent eddies are modeled. The basic assumption is that the smaller turbulent eddies are isotropic; i.e., it is assumed that the small eddies are independent of coordinate system orientation and always behave in a statistically similar and predictable way, regardless of the turbulent flow field. LES requires significantly less computer resources than does DNS, because the need to resolve the smallest eddies is eliminated in the flow field. In spite of this, the computer requirements for practical engineering analysis and design are nevertheless still formidable using today's technology.

3. **Reynolds-Averaged Navier-Stokes(RANS) Simulation** : From the averaging procedure, some terms involving the turbulent fluctuations appear (e.g., the Reynolds stress term). The effect of turbulent fluctuations must be modeled to close the system. Various turbulence models for the Reynolds stresses have been derived and used frequently in different applications. Examples of these models are the two-equation models (e.g. k-ϵ , k-ω [19], SST [20]) In RANS equation we take into account the a new term called the specific Reynolds stress tensor $\tau_{ij,turbulent}$ that translates the dissipation of energy generated by the small eddies as heat due to viscosity effect. Hence, the Navier-Stokes Equation becomes :

$$(\overrightarrow{V} \cdot \overrightarrow{\nabla}) \cdot \overrightarrow{V} = -\frac{1}{\rho}\overrightarrow{\nabla}P' + \nu\nabla^2\overrightarrow{V} + \overrightarrow{\nabla} \cdot \tau_{ij,turbulent} \tag{3.7}$$

And the stress tensor :

$$\tau_{ij,turbulent} = -\begin{pmatrix} \overline{u'^2} & \overline{u'v'} & \overline{u'w'} \\ \overline{u'v'} & \overline{v'^2} & \overline{v'w'} \\ \overline{u'w'} & \overline{v'w'} & \overline{w'^2} \end{pmatrix} \tag{3.8}$$

Where the over bar indicates the time average of the product of two fluctuating velocity components and primes denote fluctuating velocity component

While simulating the Mother Shuttle, the turbulence model employed by StarCCM+ software is **RANS k-ϵ model** that represent the turbulent flow using two terms : The kinetic energy k and the dissipation rate ϵ (Eq.3.5). Therefore, as mentioned earlier in section 3.4 when dealing with turbulent flow, additional turbulent quantities must be specified to the software, in order to calculate the kinetic energy and dissipation rate of the turbulent flow simulated. In StarCCM+ these two are : Turbulence Intensity and Turbulence viscosity ratio.

Chapter 4

CFD Winglet Validation

This chapter aims to validate the effectiveness of using winglet devices in an aircraft.
In the context of the proposed UAM cargo shuttle presented in this thesis, which features 4 wings, limited literature is available discussing the impact of having 4 winglets on aerodynamic performance. It remains unclear whether the effects are similar to those observed in normal passenger airplanes equipped with 2 winglets, or if additional factors come into play.

When an aircraft is flying, the high pressure flow beneath the wing joins the low pressure flow over the wing by generating a vortex and therefore creating undesired drag.[21] The concept of winglets, originated in the late 1800s and was later reintroduced by Dr. Richard Whitcomb in the 1970s [22], contributes in reducing drag and improving cruising efficiency in an aircraft through mitigation of vortex generation behind the wingtip. By introducing winglet devices at the wingtips, Whitcomb was able to enhance cruise efficiency from 6% to 9% .[23].

To assess the continued benefits of incorporating winglet devices in each wing of the mother shuttle cargo aircraft, three different winglet configurations were chosen for this study, differing in their cant angles as shown in the previous chapter. The selection of these angles was based on literature review, which indicated that the optimal winglet cant angles typically fall within the range of 45° to 75°, depending on flight conditions, airfoil design, and aircraft size and shape.[21]

In total, nine configurations were established and simulated using the Star-CCM+ software with a RANS k-epsilon turbulence model. The post-processing analysis focused on drag and lift performance, and a validation target function incorporating these two parameters was designed to assess the optimal configurations among the nine simulations. Additionally, a sensitivity analysis was conducted to investigate the individual effects of the front and rear winglets on drag, lift, turbulence, and vortex generation.

Furthermore, a comparison between the baseline configuration and the optimal configuration highlighted the associated benefits of winglets in mitigating vortex and turbulent structures.

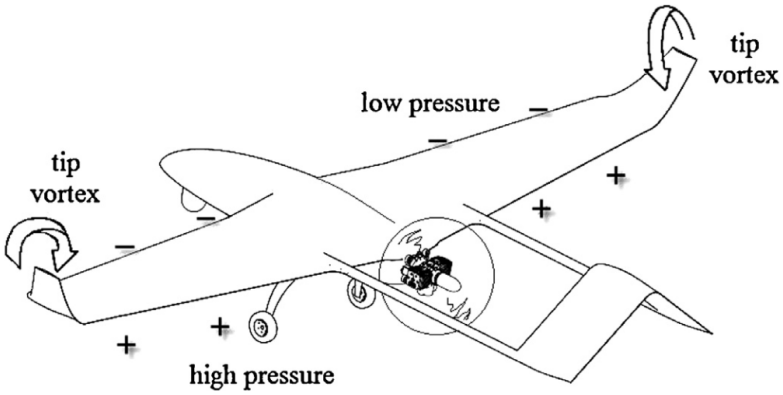

Figure 4.1: Tip vortex formation
[21]

4.1 Winglet Device

Winglets are specially designed extensions adjusted to the wingtip that alter the velocity and pressure field and reduce the induced drag term, thus increasing aerodynamic efficiency.[21]

When exposed in subsonic flow, a finite wing's drag is a combination of profile drag and induced drag. The profile drag is the drag due to the shape of the body. The induced drag is a different type of drag. It is caused by the pressure imbalance at the tip of a finite wing between its upper (pressure side) and lower (suction side) surfaces. That imbalance is necessary in order to produce a positive lift force. However, near the tip the high pressure air from the lower side tends to move upwards, where the pressure is lower, causing the streamlines to curl. This three-dimensional motion leads to the formation of a vortex, which alters the flow field and induces a velocity component in the downward direction at the wing, called *downwash*. The lift vector is tilted backwards and a force component in the direction of the drag appears, called induced drag. [21]. In commercial passenger airplanes, the lift-induced drag can amount to as much as 40% of the total drag at cruise conditions.[24] ‘

One way to reduce the lift-induced drag is by increasing the wingspan. However, increased wingspan requires strengthening the wing structure so that it can withstand the increased bending moments. Another way of reducing lift-induced drag is by using wingtip devices, such as winglets.

Winglets do not all look the same; nevertheless, their ultimate goal is always lift-induced drag reduction by artificially increasing the span of the wings.

In the case of the mother shuttle a *Blended Winglet* design have been considered as shown in Figure 4.3

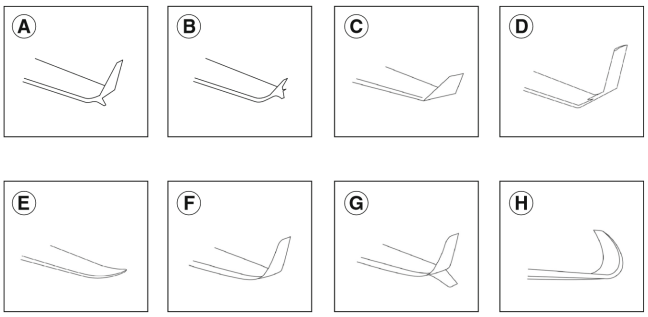

Figure 4.2: Different types of winglets and wingtip devices

(a) A Whitcomb winglet. B Tip fence. C Canted winglet. D Vortex diffuser. E Raked winglet. F Blended winglet. G Blended split. H Sharklet
[24]

4.2 Turbulence Equations Employed

As elucidated in Section 3.5, the Reynolds-Averaged Navier-Stokes (RANS) approach involves decomposing the Navier-Stokes equations for the instantaneous velocity and pressure fields into mean and fluctuating components. The resulting equations for the mean quantities are essentially identical to the original equations, except for the inclusion of an additional term known as the Reynolds stress tensor (Equation 3.8) in the momentum transport equation (Equation 3.2).

Within the STAR-CCM+ simulation framework discussed in this chapter, the standard $k - \epsilon$ RANS model is employed. This model incorporates the kinetic energy, denoted as k, and the dissipation rate, denoted as ϵ (Equation 3.5).

The $k-\epsilon$ model, introduced by Jones and Launder in 1972[25], belongs to the class of two equation models utilized in RANS simulations to represent turbulent flow. In this model, transport equations are solved for two turbulence quantities: the *Turbulence Length Scale* and the *Turbulence Intensity* (*Turbulence Level*). The corresponding field equations employed by the STAR-CCM+ algorithm are presented below:

1. *Turbulence Length Scale L* :

   Physical quantity describing the size of the large energy-containing eddies in a turbulent flow.

$$L = C_\mu \frac{k^{\frac{3}{2}}}{\epsilon} \tag{4.1}$$

   $C_\mu = 0.09$ Where C_μ is a model constant in the standard $k - \epsilon$ model.

2. *Turbulence Intensity I*

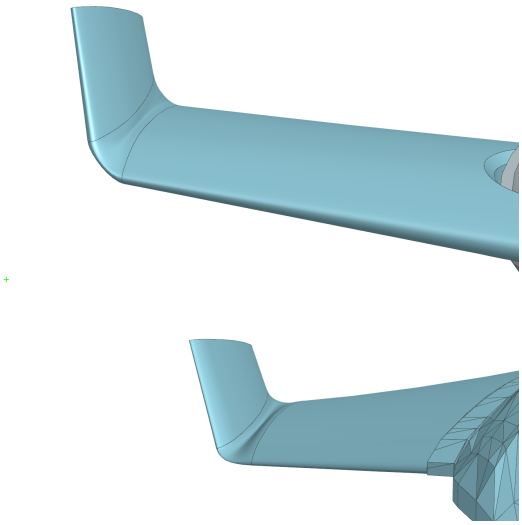

Figure 4.3: MotherShuttle Blended Winglet

$$I = \frac{\sqrt{\frac{2}{3}k}}{U} \tag{4.2}$$

Where U is the mean velocity component and k the kinetic energy that can be computed as:

$$k = \frac{1}{2}(u'^2 + v'^2 + w'^2) \tag{4.3}$$

u', v',w' are the fluctuating velocity component as represented in the Reynolds stress tensor (Equation 3.8)

4.2.1 Q-Criterion Vortexes Representation

In order to assess the effectiveness of the winglet in mitigating the generation of vortices behind the wingtip, the swirling or spinning motion of the fluid, known as vortices, is considered.
The representation and analysis of vortices is conducted using the *Q-criterion* method, a mathematical tool utilized to visualize coherent vortices within a turbulent flow. Named after the second invariant of velocity gradient vector. This method represents the balance between the vortex rotation rate, donated as Ω_{ij} and the vortex strain rate of the fluid, donated as S_{ij} Represented with the following equation :

$$Q = \frac{1}{2}\left(\Omega_{ij}\Omega_{ij} - S_{ij}S_{ij}\right) \tag{4.4}$$

Where :

- Ω_{ij} - Vortex rotational rate tensor : measures how quickly the fluid is moving in a circular or spinning motion

$$\Omega_{ij} = \frac{1}{2}\left(\frac{\partial u_i}{\partial x_j} + \frac{\partial u_j}{\partial x_i}\right) \tag{4.5}$$

- S_{ij} - Vortex strain rate tensor : refers to the measure of how much a fluid is being stretched or compressed as it flows through a vortex.

$$S_{ij} = \frac{1}{2}\left(\frac{\partial u_i}{\partial x_j} - \frac{\partial u_j}{\partial x_i}\right) \tag{4.6}$$

In the case where $Q > 0$ the vortex in detected because the strength of rotation Ω_{ij} overcomes the strain S_{ij}, making these surfaces formed by them eligible as vortex envelopes.

4.3 Drag and Lift Analysis

Configuration	Front Angle	Rear Angle	C_D	$\Delta C_D(\%)$	C_L	ΔC_L (%)
Baseline	0	0	0.3783350	0	-0.063534	0
1	45°	45°	0.3888137	-2.77	-0.0309346	51.31
2	45°	60°	0.3947795	-4.35	-0.0234275	63.13
3	45°	75°	0.4010326	-6.00	-0.0191939	69.79
4	60°	45°	0.3887983	-2.77	-0.0276590	56.47
5	60°	60°	0.3947665	-4.34	-0.0241681	61.96
6	60°	75°	0.4006631	-5.90	-0.0176130	72.28
7	75°	45°	0.3905199	-3.22	-0.0176987	72.14
8	75°	60°	0.3783350	-4.76	-0.0176310	72.25
9	75°	75°	0.4022691	-6.33	-0.0175633	72.36

Table 4.1: Drag and Lift Coefficients For the 9 Configurations

The analysis of the drag and lift trends reveals that the incorporation of winglets at the wingtips of the mother shuttle has a dual effect on its aerodynamic performance compared to the baseline configuration without winglets. While the addition of winglets improves the lift profile, it also leads to an increase in drag coefficient. However, this effect is not symmetrical, with the enhancement in lift being significantly greater than the deterioration in drag. In terms of lift, the lift coefficient experiences a substantial improvement in all wing configurations with winglets, ranging from a 51% increment in the worst configuration to varying degrees of improvement in the other configurations. On the other hand, the drag coefficient shows a maximum increase of 6.2% compared to the baseline configuration.

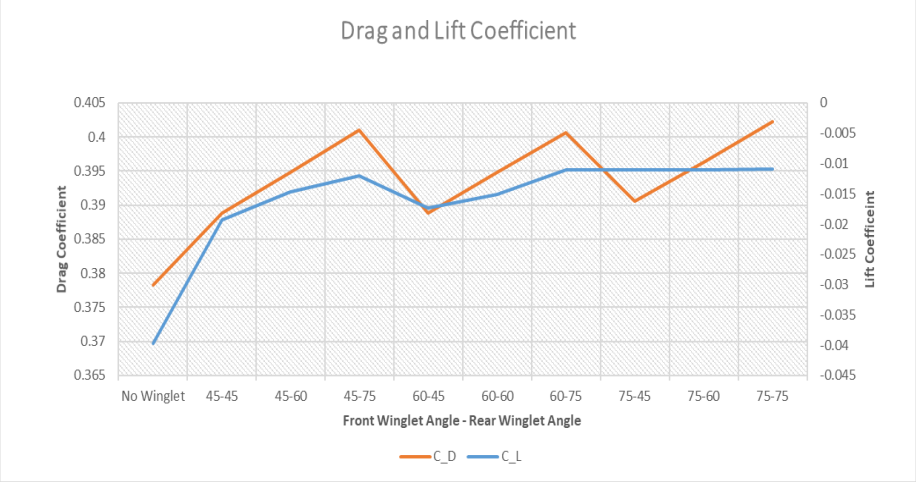

Figure 4.4: Drag and Lift coefficient rend for different winglet configuration

Interestingly, the configuration featuring a front winglet angle of 75° exhibits the worst drag profile among all the configurations, while simultaneously demonstrating a better lift coefficient. Conversely, the configurations with a rear winglet angle of 45° have the lowest drag coefficient as well as the lowest lift coefficient. As be further elaborated in section 4.4, these findings indicate that the aerodynamic performance is primarily influenced by the rear cant angle, and a conflicting trend is observed where the configuration with the best lift performance corresponds to the worst drag performance.

To further investigate the individual effects of each angle, a sensitivity analysis has been conducted. This analysis aims to study the impact of each cant angle separately and establish a validating design function to determine the optimal configuration among the nine simulated options. By evaluating the results of this analysis, a suitable winglet configuration can be selected to maximize the aerodynamic performance of the mother shuttle.

4.4 Sensitivity Analysis

The sensitivity analysis depicted in Figure 4.5 reveals that increasing the rear cant angle is associated with an increase in both drag and lift.
Increasing the rear cant angle has a negative impact on drag, as illustrated in Figure 1. For the three different front winglet angle configurations, an increase in the rear cant angle leads to a higher drag coefficient. Conversely, increasing the rear cant angle has a positive effect on lift.
Only when the front cant angle is set at 75° does the lift coefficient become

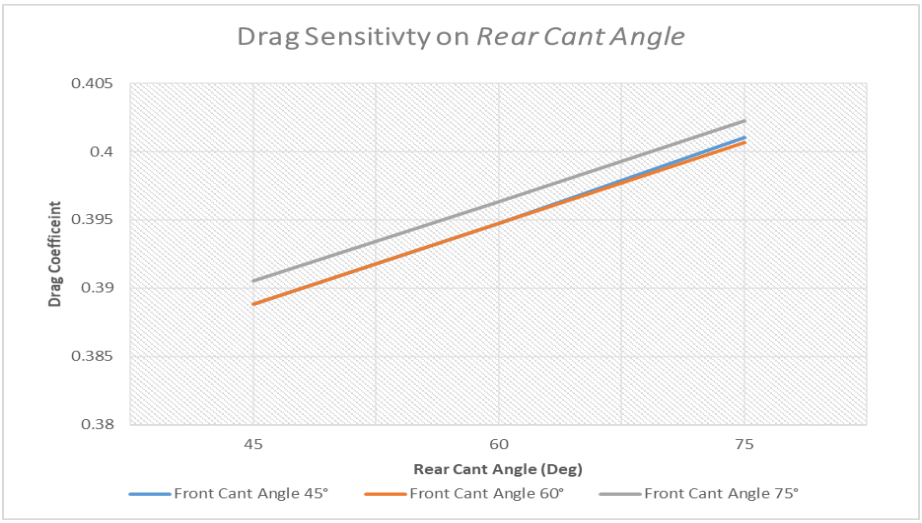

(a) Drag Coefficient

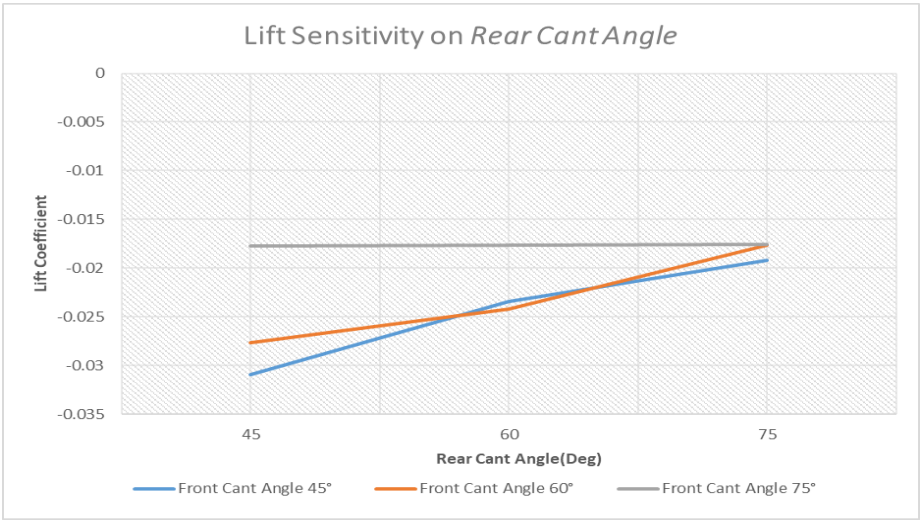

(b) Lift Coefficient

Figure 4.5: Sensitivity Analysis on *Rear Cant Angle*

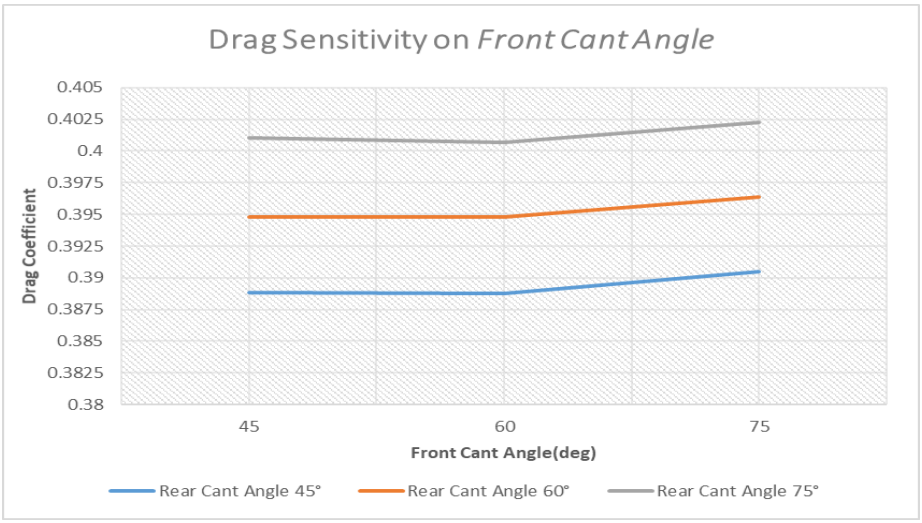

(a) Drag Coefficient

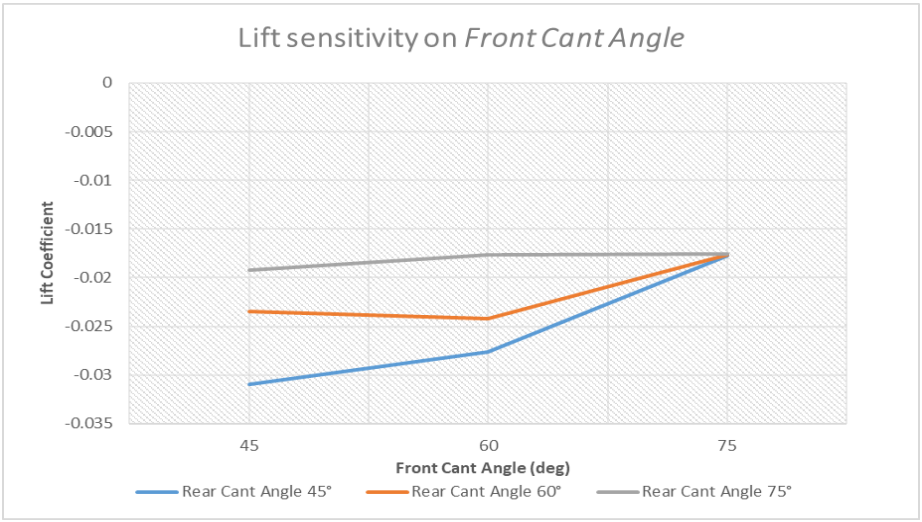

(b) Lift Coefficient

Figure 4.6: Sensitivity Analysis on *Front Cant Angle*

insensitive to the rear angle, maintaining a consistently high value.
This indicates that a front cant angle of 75° represents the optimal configuration in terms of lift but the worst configuration in terms of drag.

For the three different rear cant angle configurations, the drag slightly increases when increasing the front cant angle, making the contribution of the front winglet angle to drag much lower than that of the rear winglet angle, as shown in Figure 4.6 The drag is more affected by the rear angle than by the front cant angle, suggesting that varying the rear cant angle of the mother shuttle has a greater impact on drag than varying the front cant angle. Additionally, the drag sensitivity analysis with respect to the front cant angle reveals that the minimum drag coefficient value is obtained at a front cant angle of 60°, across all three rear winglet angle configurations, making the configuration 4 (Table 4.1) the most favorable in terms of drag profile.
It is worth noting that higher cant angles, both for the front and rear winglets, lead to increased drag generation caused by the winglet addition.

The lift sensitivity analysis with respect to the front cant angles (Figure 4.6b) also shows a general increasing trend as the front winglet angle increases. Similar to the lift sensitivity with respect to the rear cant angle(Figure 4.5b), the lift coefficient remains nearly constant at a front cant angle of 75°, where all configurations converge to the same maximum lift coefficient value. Furthermore, the values of the lift coefficient stabilizes to the maximum value whenever one of the cant angles is equal to 75°. Therefore, the 75° winglet angle configurations represent the ones with the optimal lift performance,making the configuration 9 (Table 4.1) the optimum winglet configuration in terms of lift , and signifies the point at which the front and rear angles become decoupled and independent of each other, specifically for the lift coefficient profile.

In conclusion, for the mother shuttle, the winglet cant angles of the rear wings have a greater effect on aerodynamic performance parameters such as drag (C_D) and lift (C_L). This is due to the larger area of the rear wings, which contributes more to drag generation. The analysis demonstrates that increasing the winglet angles simultaneously has a significant positive effect on lift and a moderate negative effect on drag. A 75° winglet angle configuration for both the front and rear wings stabilizes the aerodynamic performance to an optimal level, particularly in terms of lift.

4.5 Optimal Configuration

A validation target function t represented in Equation 4.7 was formulated to assess the lift and drag performance of different winglet configurations. In this target function, the lift coefficient was assigned a higher weight, surpassing the significance of the drag coefficient by a factor of 1.6. This approach facilitated the identification of an optimal winglet configuration and enabled the validation

of its effectiveness in comparison to the flat wings configuration. By prioritizing the lift coefficient, the target function ensured that the chosen winglet configuration would enhance lift performance while considering the impact on drag as well.

$$t(\alpha_1, \alpha_2) = 8C_L(\alpha_1, \alpha_2) - 5C_D(\alpha_1, \alpha_2) \tag{4.7}$$

Where α_1 and α_2 are respectively the front and rear winglet cant angle.

The prioritization of the lift coefficient over the drag coefficient in the target function serves the purpose of minimizing the downward vertical force resulting from the suboptimal wing airfoil design. This is particularly important for UAM (Urban Air Mobility) aircraft, as their lift force is primarily generated through rotors rather than traditional wings. Since UAM aircraft rely on VTOL (Vertical Takeoff and Landing) technology and do not have dedicated runways, assessing the contribution of winglets in generating lift and improving the overall lift coefficient becomes crucial in this particular application

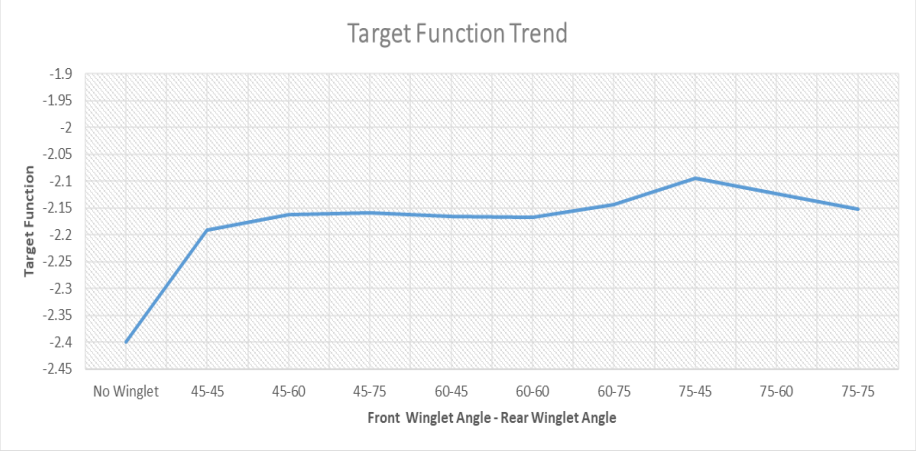

Figure 4.7: Target Function t Trend

As shown in Figure 4.7 the configuration 7 with a front cant angle of 75° and a rear cant angle of 45° has the highest value in the target function, making it the optimal winglet configuration. The configuration 9, which was previously identified as the best in terms of lift improvement, is not the optimal choice due to the higher turbulence length and vortex magnitude (Figure 4.8) near the wingtip caused by the larger rear cant angle.

Figure 4.8 illustrates the comparison of turbulence length between configuration 7, which represents the best lift performance, and configuration 9, the overall optimal configuration determined by the target function. The top figures, showing the top, midsection and side profile clearly demonstrate the disparity in turbulence length magnitude at the extremity of the rear wings. A

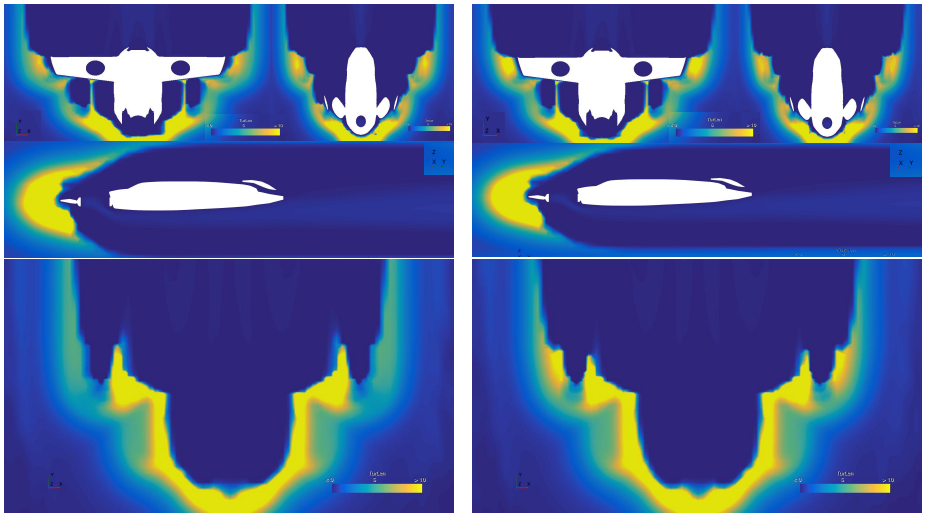

(a) $RearCantAngle = 45°$-Optimal Configuration

(b) $RearCantAngle = 75°$ - Best Lift Configiration

Figure 4.8: Turbulence Length Comparison at $FrontCantAngle = 75°$

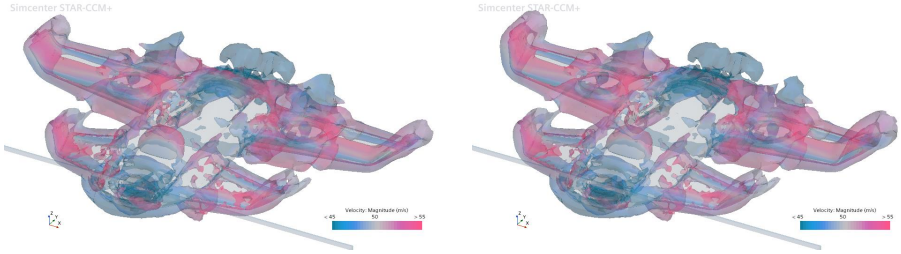

(a) $RearCantAngle = 45°$

(b) $RearCantAngle = 75°$

Figure 4.9: Q-Criterion Vortex Comparison at $FrontCantAngle = 75°$

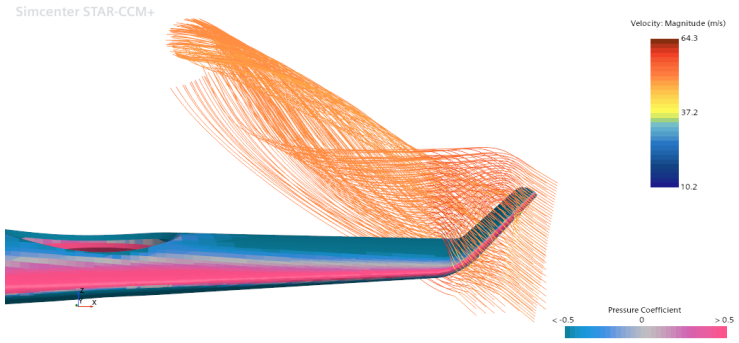

(a) Cant Angle = 45°

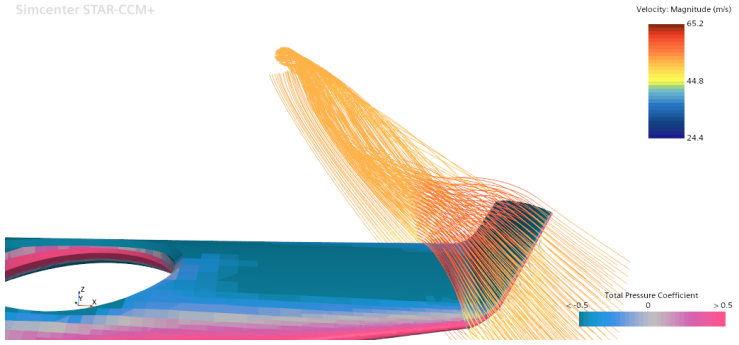

(b) Cant Angle = 60°

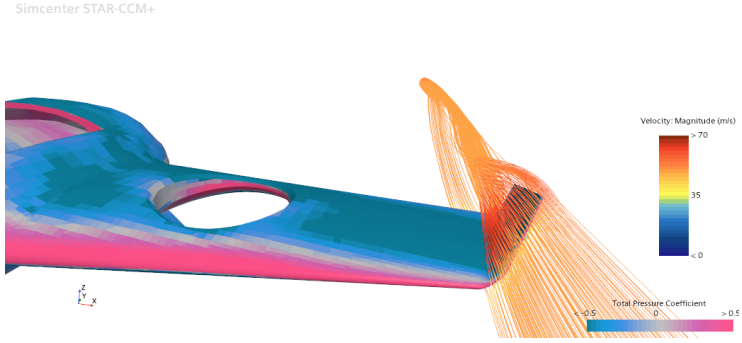

(c) Cant Angle = 75°

Figure 4.10: Velocity Field Streamlines for 3 different cant angles

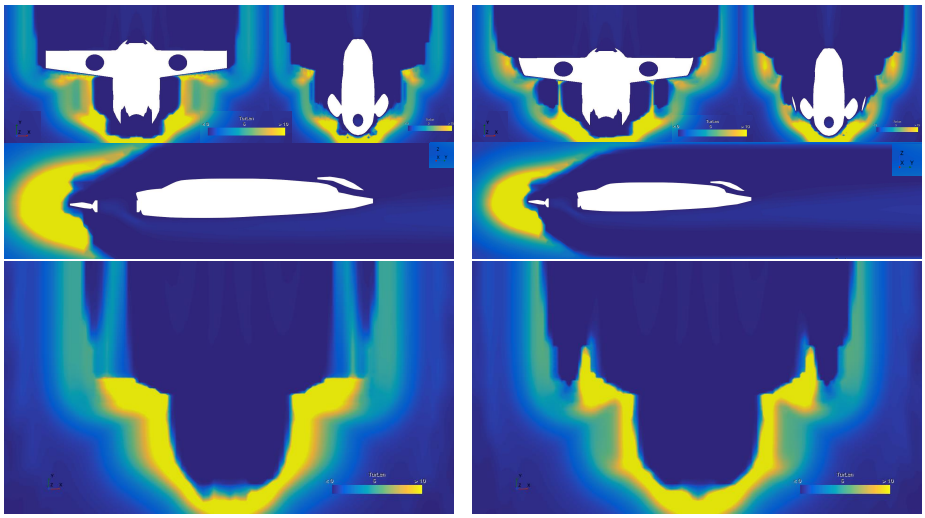

(a) Baseline Configuration (b) Optimal Configuration

Figure 4.11: Turbulence Length Comparison at between baseline and optimal configuration (N°7)

higher rear cant angle led to a greater turbulence length. This observation is further supported by the bottom figures in Figure 4.8, which display the turbulence length along the lower profile of the mother shuttle (projection on the Z-axis). The transition from yellow to blue at the winglet position indicates a reduction in turbulence length from 10 to less than 5. This reduction signifies that a lower rear cant angle mitigates turbulence structures near the wingtip, whereas a higher cant angle introduces larger turbulence structures. Consequently, configuration 9, despite its superior lift performance, is not the optimal configuration as the increased turbulence structures contribute to higher drag generation, as explained in section 4.4. This ultimately diminishes its value in the target function t. The mathematical formulation of turbulence length is given by equation 4.1.

Figure 4.9 presents another aspect of the flow behavior around the wing's extremity, focusing on the q criterion vortex. Comparing the two configurations, it is evident that at a higher rear winglet angle, the magnitude of the vortex increases. This observation aligns with the increase in drag generation experienced for all configurations with a rear winglet angle of 75°, as shown in Figure 4.7.

4.6 Comparison with baseline

This section compares the optimal configuration with the baseline configuration of the Mother Shuttle UAM aircraft. The focus is on analyzing the turbulence

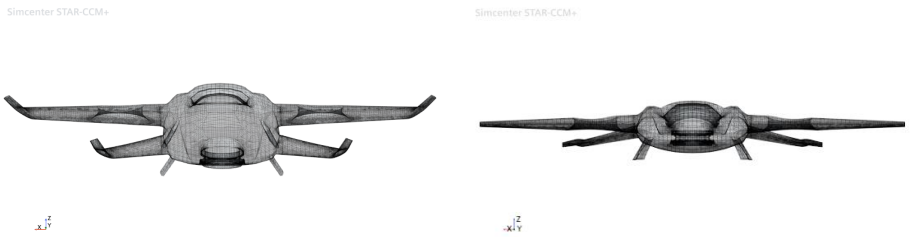

(a) Optimal Configuration (b) No winglet

Figure 4.12: Optimal Winglet Configuration external shape versus Baseline

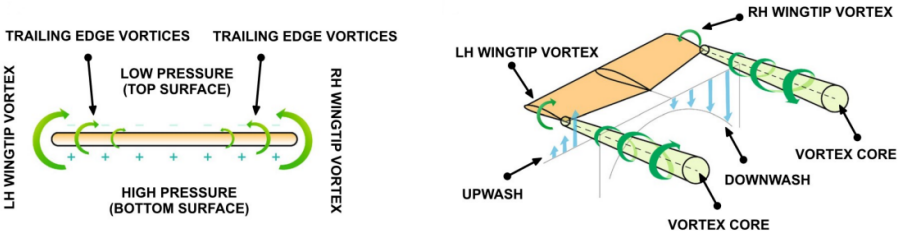

Figure 4.13: Wingtip vortices and associated downwash [21]

behavior of the flow around the aircraft and examining the lift and drag development profiles.

As the primary objective is to validate the effectiveness of incorporating winglet devices in a 4-wing structure aircraft, this study aims to demonstrate that the addition of winglets can lead to overall improvements in aerodynamic performance, albeit in a different manner compared to traditional passenger airplanes with 2 winglets.

Figure 4.11 compares the turbulence length between the baseline and optimal configurations. In the optimal configuration, a notable improvement can be observed near the two rotors, where the turbulence length is reduced to zero. Additionally, the top profile demonstrates a decrease in turbulent flow behind the winglet, indicating a reduction in vortex generation behind the wingtip.

In a flat wings configuration, the so called *wingtip vortices* illustrated in figure 4.13, also known as *trailing edge vortices*,where the flow curles and high velocities and low pressure exist at their cores, result in a downward flow in the neighborhood of the wing known as the *downwash*. This *downwash* interacts with the free stream velocity to induce a local relative wind deflected downward in the vicinity of each airfoil section of the wing. The winglet device mitigates the strength of these vortices, thereby reducing the average wing *downwash*.[21]

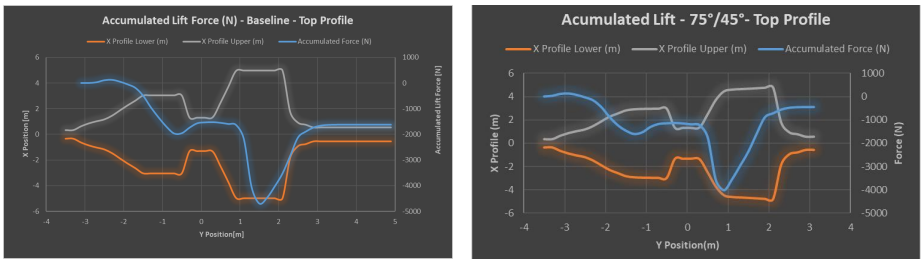

(a) Baseline (b) Optimal Configuration

Figure 4.14: Lift Profile comparison with respect to the optimal configuration

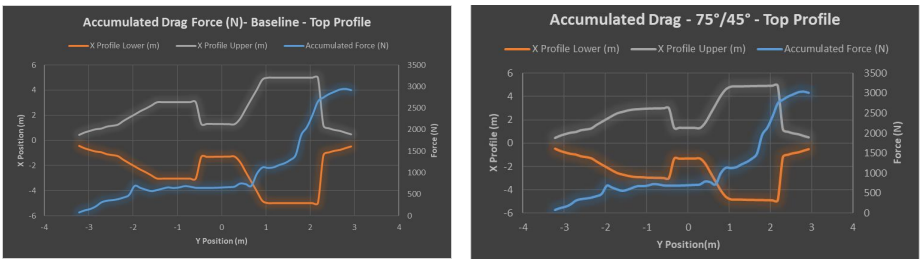

(a) Baseline (b) Configuration 7

Figure 4.15: Drag Profile comparison with respect to the optimal configuration

In the case of the Mother Shuttle, this *downwash* mitigation leads to a significant 72% improvement in lift coefficient compared to the baseline configuration(Table 4.1). The accumulated lift profiles in the figure 4.14 further illustrate this improvement. The accumulated downward force in the baseline configuration is reduced from approximately 1500N to less than 500N in magnitude. The lift recovery is particularly notable at specific positions along the aircraft where the winglets are incorporated. At Y = -0.5m, which corresponds to the end of the front winglet, a significant lift recovery of 800N is observed in configuration 7 compared to the baseline. Furthermore, at the end of the rear winglet (Y = +2m), the lift recovery reaches 2500N.

As highlighted in table 4.1, all the winglet configurations resulted in an increase in drag generation, with the optimal configuration showing a 3% increase. This increase in drag can be attributed to the turbulent flow observed in the wings' extremities, as shown in figure 4.11. The projection on the Z axis reveals an expansion of the turbulent region after incorporating the winglet.
This increase in turbulent flow contributes to an accumulation of drag force at this specific location of the shuttle. A slight augment in accumulated drag force can be observed at the end of the rear wing (Y=+2m) in figure 4.15.

Figure 4.16 provides a comparison of the velocity flow field at the wingtip between the optimal winglet configuration and the baseline configuration. With-

out the winglet, the streamlines exhibit significant swirling motion and a strong tip vortex. However, the presence of the winglet straightens the streamlines, reducing the intensity of the swirling fluid motion. This demonstrates the effectiveness of the winglet in mitigating the tip vortex and reducing the downward lift-induced drag force, as depicted in Figure 4.14. Furthermore, Figure 4.10 shows that increasing the cant angle of the winglet further reduces flow separation and the wingtip vortex.

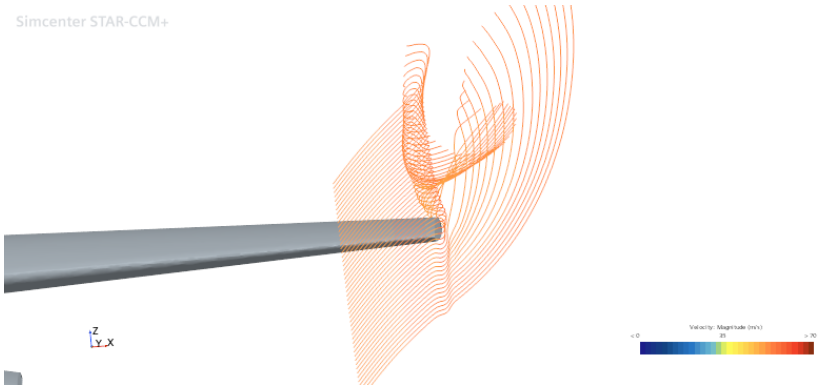

(a) Baseline

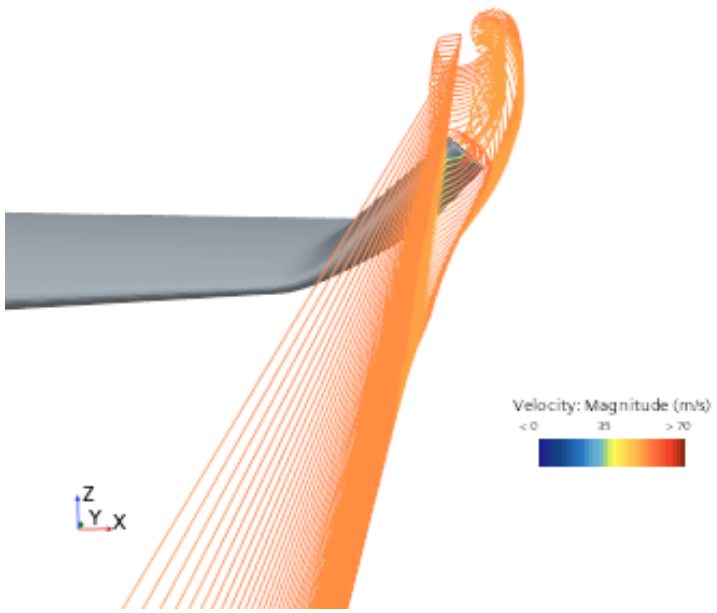

(b) Optimal Configuration

Figure 4.16: Rear Wing Tip Vortex Comparison between baseline and optimal configuration

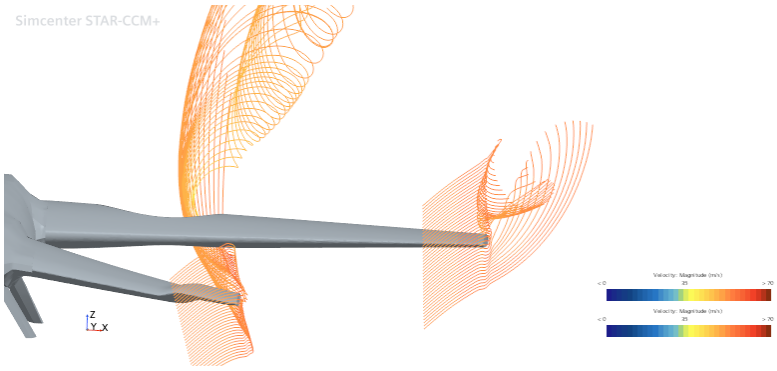

(a) Baseline

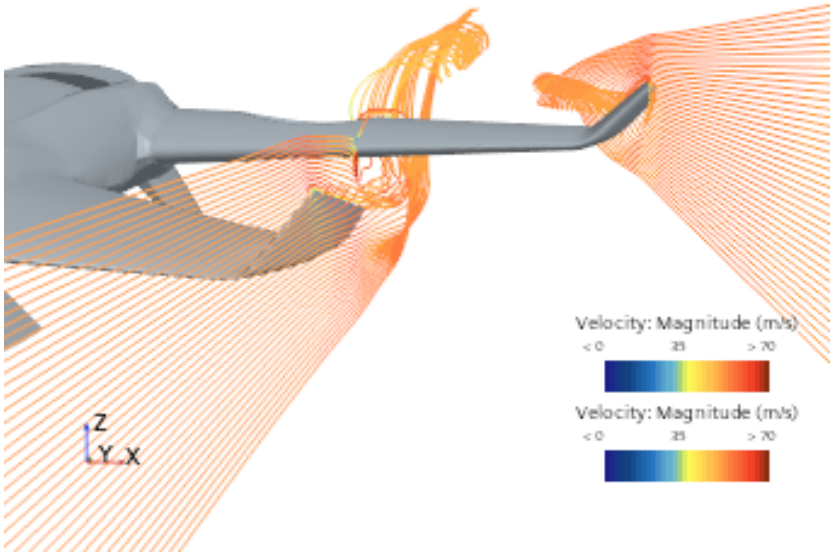

(b) Optimal Configuration

Figure 4.17: Tip Vortex for the two wing tip

Chapter 5

Conclusion and discussion

The aim of this thesis was to propose a futuristic solution, the Mother&Baby Drones Shuttle (MbdS), to address the challenges associated with last-mile deliveries, particularly in suburban areas. The solution, developed in collaboration with engineers and designers for the IDEEA 2023 international future mobility solution design contest, integrates Urban Air Mobility technology to provide sustainable and efficient parcel delivery services. The solution was elaborated along with the design of the whole delivery scenario, encompassing future warehouse planning, integration of the aerial delivery module, sustainable parcel packaging, and smart aerial final handing over to the user by air drop. This comprehensive upgrade of the last mile delivery processes serves the goal of achieving a seamless and environmentally-friendly parcel delivery experience.

The second part of the thesis focused on the CFD validation of the main aerial platform responsible for cargo transport, specifically investigating the aerodynamic performance improvement achieved through the incorporation of winglet devices. Winglets have long been known for their potential to reduce induced drag and improve aerodynamic efficiency. The study utilized StarCCM+ software to simulate and compare different winglet configurations, ultimately selecting an optimal configuration based on a target function considering lift and drag coefficients The geometry of 3D shuttle Model have been defined. Three different winglet configuration differing in their cant angle have been generated resulting of in total 9 winglet-featured configurations.

The findings revealed an opposing trend between drag and lift profiles, indicating that winglet-featured configurations that enhanced lift coefficient simultaneously increased drag coefficient. Additionally, increasing the cant angles of the winglets reduced tip vortex formation and streamlines curling phenomena associated with flat wing configurations. However, at higher cant angles, a slight increase in drag was observed. Notably, the effect of the rear wings and rear winglet angle on drag was more pronounced than that of the front wings and front winglet angle.

The study demonstrated that the impact of having four winglets on the aerodynamic behavior of the aircraft differed from that of having two winglets. The latter configuration primarily improved cruising efficiency and reduced drag by minimizing the downward force associated with lift-induced drag and tip vortex. Conversely, the former configuration significantly enhanced lift while moderately compensating for drag coefficient. Therefore, the addition of winglet devices has the potential to greatly improve the aerodynamic performance of future four-wing aircraft. Further research could explore optimizing the winglet's airfoil shape to maximize its drag-reducing benefits while minimizing overall drag.

In conclusion, the successful implementation of the proposed last mile delivery solution relies on the development of a future city environment that encompasses aerial urban vehicles for passenger and cargo transport. This solution offers the potential to enhance delivery speed, reduce traffic congestion, and automate warehouse operations from parcel allocation to final delivery by baby drones. However, its feasibility depends on the integration of urban air transport and the establishment of advanced infrastructure in future distribution centers. This infrastructure must not only ensure safe takeoff and landing but also facilitate the seamless integration of the mother shuttle and baby drones within warehouse operations and define their efficient interaction with warehouse parcels.
Further research should focus on designing warehouse environments specifically tailored for aerial cargo delivery, while also considering user adaptability to air drop deliveries in a future city setting.

Bibliography

[1] L. Pugliese, F. Guerriero, and G. Macrina. Using drones for parcels delivery process. *Procedia Manufacturing*, 42:488–497, 2020.

[2] Capgemini. The last-mile delivery challenge: Giving retail and consumer product customers a superior delivery experience without impacting profitability. Technical report, Capgemini, 2018.

[3] S. Srinivas, S. Ramachandiran, and S. Rajendran. Autonomous robot-driven deliveries: A review of recent developments and future directions. *Transportation Research Part E: Logistics and Transportation Review*, 165:102834, September 2022.

[4] China Labour Bulletin. Fatal accident highlights intense pressures faced by China's food-delivery workers, December 2017.

[5] K. O. Ploetner and Al Haddad et.al. Long-term application potential of urban air mobility complementing public transport: an upper Bavaria example. *CEAS Aeronautical Journal*, 11(4):991–1007, December 2020.

[6] A. Straubinger, R. Rothfeld, M. Shamiyeh, K.D. Büchter, J. Kaiser, and K.O. Plötner. An overview of current research and developments in urban air mobility – Setting the scene for UAM introduction. *Journal of Air Transport Management*, 87:101852, August 2020.

[7] Study on the societal acceptance of Urban Air Mobility in Europe. Study, EASA : European Union Aviation Safety Agency, May 2021.

[8] O. Dedehayir and M. Steinert. The hype cycle model: A review and future directions. *Technological Forecasting and Social Change*, 108:28–41, July 2016.

[9] A.H. Michel. Amazon's drone patents. In *dronecenter.bard.edu*, pages 7–8, September 2017.

[10] P. Kotler and G. Armstrong. *Principles of marketing.* Pearson Higher Education, Hoboken, seventeenth edition edition, 2018.

[11] A.F. Marique and S. Reiter. A method for evaluating transport energy consumption in suburban areas. *Environmental Impact Assessment Review*, 33(1):1–6, 2012.

[12] C.E. Kunkel. The Effect of Grocery Delivery Services on Last Mile Emissions. 2020.

[13] J. Alba-Maestre, K. Prud'homme Van Reine, T. Sinnige, and S.G.P. Castro. Preliminary Propulsion and Power System Design of a Tandem-Wing Long-Range eVTOL Aircraft. *Applied Sciences*, 11(23):11083, November 2021.

[14] B. German, M. Daskilewicz, T. K. Hamilton, and M. M. Warren. Cargo Delivery in by Passenger eVTOL Aircraft: A Case Study in the San Francisco Bay Area. In *2018 AIAA Aerospace Sciences Meeting*, Kissimmee, Florida, January 2018. American Institute of Aeronautics and Astronautics.

[15] Y.A. Çengel and J.M. Cimbala. *Fluid mechanics: fundamentals and applications*. McGraw Hill, New York, third edition edition, 2014.

[16] D.C. Wilcox. *Turbulence Modelling for CFD*. 3rd edition, November 2006.

[17] L.F. Richardson and P. Lynch. *Weather Prediction by Numerical Process*. Cambridge Mathematical Library. Cambridge University Press, 2 edition, 2007.

[18] T. Poinsot and D. Veynante. Theoretical and numerical combustion. *Prog. Energy Combust. Sci.*, 28, 01 2005.

[19] B. E. Launder. Turbulence modelling for cfd. by d. c. wilcox. dcw industries inc., 1993. 460pp. 75. *Journal of Fluid Mechanics*, 289:406–407, 1995.

[20] F. Menter, M. Kuntz, and R.B. Langtry. Ten years of industrial experience with the sst turbulence model. *Heat and Mass Transfer*, 4, 01 2003.

[21] P. Panagiotou, P. Kaparos, and K. Yakinthos. Winglet design and optimization for a MALE UAV using CFD. *Aerospace Science and Technology*, 39:190–205, December 2014.

[22] M. Curry. NASA Dryden Technology Facts - Winglets, March 2008.

[23] M. Segui, F.R. Abel, R. M. Botez, and A. Ceruti. New Aerodynamic Studies of an Adaptive Winglet Application on the Regional Jet CRJ700. *Biomimetics*, 6(4):54, September 2021.

[24] J. E. Guerrero, M. Sanguineti, and K. Wittkowski. Variable cant angle winglets for improvement of aircraft flight performance. *Meccanica*, 55(10):1917–1947, October 2020.

[25] W.P. Jones and B.E. Launder. The prediction of laminarization with a two-equation model of turbulence. *International Journal of Heat and Mass Transfer*, 15(2):301–314, February 1972.